The osmotic demyelination syndrome

Gilloteaux, Jacques; Bouchat, Joanna; Brion, Jean Pierre; Nicaise, Charles

Published in:
Ultrastructural Pathology

DOI:
10.1080/01913123.2020.1853865

Publication date:
2020

Document Version
Peer reviewed version

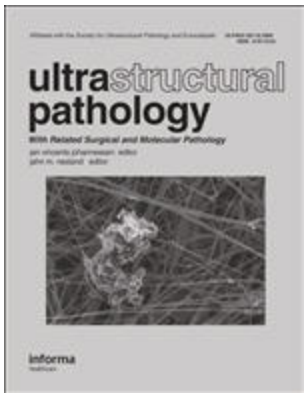

The osmotic demyelination syndrome: the resilience of thalamic neurons is verified with transmission electron microscopy.

Journal:	*Ultrastructural Pathology*
Manuscript ID	UUSP-2020-0090.R1
Manuscript Type:	Original Papers
Date Submitted by the Author:	n/a
Complete List of Authors:	Gilloteaux, Jacques; St George's University School of Medicine, Anatomical Sciences; Universite de Namur, Faculty of Medicine- Unite de Recherche en Physiologie Moleculaire Bouchat, Joanna; Universite de Namur, Unite de Physiologie Moleculaire URPhyM - NARILIS Brion, Jean-Pierre; Universite Libre de Bruxelles Faculte de Medecine, Laboratory of Histology, Neuroanatomy and Neuropathology Nicaise, Charles; Universite de Namur, Faculty of Medicine- Unite de Recherche en Physiologie Moleculaire
Keywords:	Thalamus, Neuron, Cell body, Nucleolus, Osmotic demyelination syndrome, Restoration

The osmotic demyelination syndrome: the resilience of thalamic neurons is verified with transmission electron microscopy.

Jacques Gilloteaux [1, 3], Joanna Bouchat [1], Jean-Pierre Brion [2], Charles Nicaise [1]

[1] Unit of Research in Molecular Physiology (URPhyM- NARILIS), Department of Medicine, Université de Namur, 61, rue de Bruxelles, B- 5000 Namur, Belgium.

[2] Laboratory of Histology, Neuroanatomy and Neuropathology, Faculté de Médecine Université Libre de Bruxelles, 808 route de Lennik, B- 1070 Brussels, Belgium.

[3] Department of Anatomical Sciences, St George's University School of Medicine, KB Taylor Global Scholar's Program at UNN, School of Health and Life Sciences, Drill Hall 013, Newcastle upon Tyne NE1 8JG, United Kingdom.

Abstract

The development of a murine model of osmotic demyelinating syndrome (ODS) allowed to study changes incurred in extrapontine zones of the CNS and featured neuron and glial cell changes in the relay thalamic ventral posterolateral (VPL) and ventral posteromedial (VPM) nuclei before, during and after ODS induction, and characterized without immune response. There, the neuron Wallerian-type deteriorations were verified with fine structure modifications of the neuron cell body, including some nucleus topology and its nucleolus changes. Morphologic analyses showed a transient stoppage of transcriptional activities while myelinated axons in the surrounding neuropil incurred diverse damages, previously reported. Even though the regional thalamus myelin deterioration was clearly recognized with light microscopy 48h after osmotic recovery of ODS, ultrastructure analyses demonstrated that, at that time, the same damaged parenchyma regions contained nerve cell bodies that have already reactivated nucleus transcriptions and neuroplasm translations because peculiar accumulations of fibro-granular materials, similar to those detected in restored ODS astrocytes, were revealed in these restructuring nerve cell bodies. Their aspects suggested to be accumulations of ribonucleoproteins. The findings suggested that progressive neural function's recovery in the murine model could imitate some aspects of human ODS recovery cases.

Running title: ODS thalamus and neuron cell bodies

Key words: Murine – thalamus – neuron – cell body - nucleus – nucleolus - ultrastructure – osmotic demyelination syndrome – cell injury – restoration –

Corresponding author:
Dr J Gilloteaux, URPhyM- NARILIS, Université de Namur, Département de Médecine, rue de Bruxelles 61, B- 5000 Namur, Belgium; Email jacques.gilloteaux@unamur.be and Department of Anatomical Sciences, St George's University School of Medicine at UNN-School of Life Sciences, Northumberland Road, 013 Drill Hall, NE1 8JG Newcastle upon Tyne, United Kingdom; Email: jagilloteaux@sgu.edu

"*Fortiter defendit triumphans*" ('Triumphing by brave defence')
[Motto of Newcastle upon Tyne, UK]

Introduction

The osmotic demyelination syndrome (ODS) encompasses a non-inflammatory neuropathology of broad symptomatology: from disorientation, slight confusion, paresis, deafness, memory loss to seizure, unresponsiveness and coma, depending on the degree of myelin loss in the brain distributed as 'central pontine myelinolysis' (CPM) and 'extrapontine myelin' (EPM) lesions [1-8] with EPM preceding those of CPM [9-11]. Possibly, human EPM cases seemed more frequent than CPM [12]. Furthermore, the percentage of patients involved with ODS has increased recently due to a more frequent magnetic resonance imaging (MRI) utilization in clinical settings [10, 13-23].

Chronic hyponatremia with subsequent ODS can occur in diverse conditions as soon as homeostatic level of [Na+] is perturbed [24-28] and can be more frequent in aging population [29]. In the old and current literature, number of reports of regional CPM and EPM ODS defects showed as consequences of abrupt adjustment of a temporary or chronic deficiency of the homeostatic sodium gradient. Its etiology can be found in a series of diverse afflictions [30], such as in these exemplary list of clinical studies: alcoholism and/or combined with malnutrition [1, 19, 31-40], craniofacial and neurosurgeries [41-42], diarrhoea with AIDS [43], excessive vomitus alone [44] or associated with pregnancy [45-46], hyper glycemia [47], paediatric diabetes [48], diabetes insipidus due to cancer treatments [49, folate deficiency and kidney defect [50], Grave's disease [51], diuretic unbalance and heart failure [52-55], heat exhausting exercise [56-57], liver cirrhosis [58- 59] or liver transplantation [29, 60- 61].

Disorders of sodium and osmotic homeostasis have been found in diverse small mammals [62-63]. Laboratory rats and dogs have traditionally been the species used in ODS research studies [64-67]. The development of genetically modified mouse models has hinted a way for

the manipulation of genes or cells possibly relevant to the pathophysiology of ODS. Insofar, three other studies have tried to create rodent models of ODS [68-71]. In the present paradigm, mice were experimentally subjected to chronic severe hyponatremia and then abruptly corrected allows to comfort the other published studies on this developed model of osmotic demyelinating syndrome (ODS) where changes were found in several CNS CPM and EPM regions, where containment and repairs were focused on the relay ventral posterolateral (VPL) and ventral posteromedial (VPM) thalamic nuclei. There, the susceptibility toward osmotic-induced demyelination as ODS was triggered by astrocytes signals from the osmolyte stress to oligodendrocytes allowed some responses of microglial cells and myelinolysis without incurring neuron cell death [72-74].

The aims of this report specifically focused on neuron' s cell body changes the same areas, i.e. the ventral posterolateral (VPL) and ventral posteromedial (VPM) relay nuclei, during and after ODS by using morphology techniques, with emphasis on electron microscopy aspects. The morphology of these murine thalamic relay areas was illustrated by endured neuron changes in demyelination with some distal extension excisions of the Wallerian type where no nerve cell death had occurred. During the treatment, some internal strategy revealed changes of the nucleoplasm and its nucleolus that comforted some slowed down or even hiatus or stoppage in nerve cell bodies of their transcriptional and translational activities. Those functions appeared reinstated as soon as 48h following rebalancing the physiologic environmental natriuremia. The collected data comforted the cell's survival adjustments compared to those of the macroglial and microglial cells of the myelinolytic areas of the thalamus of the same ODS readjustment periods studied and described in the aforementioned contributions [72-74]. These ultrastructure data can complete or resembled the clinical resolution observed with osmotic resolution noted in recent clinical findings [75] but where, in some cases, the clinical treatment and resolution is still uncertain [76-78]. Furthermore, our observations certainly open for further studies to understand and verify as to how neuron along with neuroglial plasticity would further restore functions of those susceptible CNS regions.

Materials and Methods

a. The animals

Male C57bl/6J mice, aged from 3 to 4 months were kept in the University Animal Facility according to the experimental ODS protocol was conducted in compliance with the European Communities Council Directives for Animal Experiment (2010/ 63/EU, 86/609/EEC and 87–848/EEC), approved by the Animal Ethics Committee of University of Namur (ethic project number 14–210).

b. The murine ODS protocol

ODS induction was based on the correction of a chronic hyponatremia, according to an adapted protocol from [67], as described in [72-73]. Briefly, an osmotic minipump (Model 1004, Alzet, Cupertino, CA) was filled with desmopressin acetate (2 µg/ml; Minirin, Ferring, Saint-Prex, Switzerland) and inserted subcutaneously under anaesthesia into the back of animals at day 0. Standard pellets and water were switched to a low-sodium liquid diet (AIN76A, MP Biomedicals, Santa Ana, CA), given ad libitum for the whole duration of hyponatremia. At day 4, hyponatremia level and serum sodium were increased back to normonatremia using a single intraperitoneal injection of NaCl 1M (1.5 ml/100 g body weight). Minipumps were left into animals until the end of experiments. Unless otherwise specified, any procedure involving anaesthesia was performed using intraperitoneal injection of a cocktail of ketamine 100 mg/kg and xylazine 5 mg/kg.

c. Experiment groups:

This fine structure investigation complements others made with neurophysiology, histology and immunohistochemistry where four groups were used (Fig 1): Group 1 were normonatremic mice (NN; n=2) sacrificed at day 0; Group 2 were hyponatremic mice (HN; n=2) sacrificed 4 days after the induction of hyponatremia (day 0 + 4-day treatment period) of 'chronic hyponatremia' as described in the ODS protocol. Groups 3 and 4 were mice which underwent the 4-day 'chronic hyponatremia' abruptly provided with normonatremia as both ODS Groups., i.e. Group 3 included mice sacrificed 12h after this fast restoration of normal natremia, thus named ODS 12h group (ODS12h; n=3) while Group 4 mice encompassed mice sacrificed 48h post osmotic correction hence named ODS48h (n=3).

d. Light microscopy (LM) and immuno-histochemistry

Under anaesthesia, all the mice were exsanguinated and perfused transcardially with warm NaCl 0.9% followed by phosphate-buffered 4% paraformaldehyde (PFA). Brains were removed, divided into two hemispheres and post fixed overnight in the same PFA fixative solution.

For histology, brains were then dehydrated, paraffin-embedded and sectioned into 6 µm thick microscopic preparations that were stained with hemalum and chromoxane cyanine R or Eriochrome C for general topographic observation of nuclei and myelin [79-80].

For immune-histochemistry, a general processing was followed according to Sternberger [81]. The paraffin sections were dewaxed, rehydrated and heat-induced antigen retrieval was performed in citrate buffer pH 6 at 100ºC for 10 minutes. Endogenous peroxidase was quenched using 3% H_2O_2 in methanol for 10 min. Non-specific binding was blocked using 5% horse or goat serum diluted in Tris-buffered saline (TBS) for 15 min. In order to characterize

neurons, sections were then incubated overnight at 4°C with NeuN primary antibodies diluted (1:1000, Cell Signaling D3S3I, Leiden, The Netherlands) in TBS containing 1% normal serum, overnight at 4ºC. Then, sections incubated with a biotinylated secondary antibody (1:100, Vectastain, Vector Laboratories, Burlingame, CA) for 1 hr at room temperature and contrasted peroxidase-bound streptavidin (1:100; Vectastain) for 45 min. Revelation was done using diaminobenzidine substrate (Dako, Glostrup, Denmark). Finally, sections were counterstained with hemalum, dehydrated and mounted in DPX. Sections were observed with an Olympus BX63 microscope (Olympus, Tokyo, Japan) equipped with Hamamatsu Orca-ER camera and images were acquired with the Cell Sens software.

e. Electron microscopy

Under anaesthesia, mice were perfused transcardially with a solution of PFA 2% and glutaraldehyde 2% in 0.1 M phosphate buffer (pH 7.4). Selected brain regions were harvested and post-fixed in glutaraldehyde 4% for 2 hr. Thalamus ventral posterolateral (VPL) and ventral posteromedial (VPM) thalamic regions were dissected (Fig. 1b) and VPM and VPL nuclei were sampled (lateral plans 1.0 to 2.0 mm from interhemispheric fissure) according to the mouse brain atlas of Franklin and Paxinos [82]. Samples were harvested using a neurological punch of 0.69 mm of internal diameter (Fine Science Tools #18036-19, Heidelberg, Germany). Tissues were washed in Millonig's buffer containing 0.5% sucrose for 24 hr and were then post-fixed in OsO4 2%, dehydrated and finally embedded in epoxy resin. Semi-thin sections were stained with toluidine blue to choose selected regions of interest for fine structure analyses. Ultrathin grey sections (ranging from 40 to 70 nm) of these regions, obtained with a diamond knife, collected on 200 and 300 mesh nickel grids (Micro to Nano, Haarlem, The Netherlands) and contrasted with uranyl acetate and lead citrate were observed with a Philips Tecnai 10 electron microscope, at an accelerating voltage of 60-80 kV, equipped with a digitized Olympus ITEM platform MegaView G2 image analysis.

Results

1. Light microscopy (LM):

a. Myelin and ODS:

Figure 2 A-D is a pane of microscopic anatomy of mice NN, HN, ODS 12h and ODS 48h brain sections stained with haematoxylin and Eriochrome C. The damaged thalamus region in ODS48h treated mice was poorly stained compared with those of NN, HN and ODS12h thalami where no obvious difference of myelin staining was observed with LM. The ODS 48h section revealed the entire zone had undergone myelinolysis at that stage, post HN treatment,

said as after chronic hyponatremia, and fast readjusted to normonatremia; this is when LM showed recognizable histopathological damages.

b. LM and NeuN immunolabeling

The NeuN marker labelled all the neurons of the sections of the ventral posterior thalamic nucleus from NN-, HN-, ODS12h- and ODS48h-treatments. Albeit of similar thickness, each showed difference in the NeuN contrast while hemalum stained nuclei, including those of macroglia, noted as satellite oligodendrocytes and highlighted in the examples inserted of each treatment in the same pane, Figure 3. At first glance, ODS12h treated thalamic sections contained cell bodies with the highest labelling intensity for NeuN of the detected marker and, following a qualitative review of the faint to strong brownish hue. One evaluated semi-qualitatively NeuN contrasts between treatments to be in the sequence: ODS12h > NN = ODS48h > HN. It is noteworthy to indicate that if ODS12h showed the highest contrast among all, the nuclei bore a poor NeuN label as they appeared with large emptied patches across the nucleoplasm while all other treatments revealed a diffused cell body immunostained pattern that encompassed nucleus and neuroplasm.

c. LM of Semi-thin epoxy sections

In both the ventral posterolateral (VPL) and ventral posteromedial (VPM) thalamic regions (the ventral posterior nucleus) 1-µm semi-thin sections stained with toluidine blue, Sham or NN neuron cell bodies were easily recognized from the neuroglial cells (Fig 4 NN, HN, ODS12h and ODS48h). The neuron somata were usually the largest sized cells, round to oblong that ranged between 9.0 to 12.5 µm in diameter; they contained a large, poorly-contrasted nucleus (7.5 to 11 µm in diam.). The large nuclei were often creased against a pale basophil neuroplasm that displayed a highly-contrasted but wide nucleolus against a faint metachromatic perikaryon due to some glycogen content. Although, following HN and ODS12h treatments, cell bodies did not demonstrate obvious damage under LM examinations, a definite rounding or shrinking compacted aspect were noted for most nucleoli in both HN and ODS12h treatments. On the opposite, ODS48h treated nuclei appeared to reveal NN features, including the topology of invaginated nucleolemma showing grooves and even some basophilia throughout the neuroplasm. This contrasted with the histologic, paraffin preparation where the ODS48h overall damage was observed by paler staining in the Eriochrome-stained sections of Figure 2, likely caused by an overall myelinolytic detection. Thus, if all the light microscopic preparations originated from NN, HN, ODS 12h and ODS 48h demonstrated nucleus and perikaryon changes, one had to survey these findings with fine structure analyses in order to verify what type(s) of ultrastructural modifications had been taken place in the thalamus where neurons have endured some Wallerian degeneration by

hyponatremia and its rapid rebalancing. Following ODS, the features detected in each of the treatment became interesting in spite of the ODS 48h cell bodies to appear in many aspects similar to NN nuclei while adjacent surrounding structures featured some remained degradations (Fig 4 ODS48h).

2. Ultrastructural aspects

The fine structure observations here reported concerned both the ventral posterolateral (VPL) and ventral posteromedial (VPM) thalamic nuclei cell bodies. There, most are interneurons whose neuropil contain long entwined neurite's extensions undergoing ODS myelinolysis, i.e. axons, dendrites and neuroglial structures that were investigated in other studies [72-74]. It is also clear that, at ODS12h, the ultrastructure examination allowed to verify the demyelinating zones along with the surrounded intact region of the thalamus nuclei while LM aspects were not entirely able to show the fine changes whether damaged, undamaged or undergoing repairs. For each treatment, several examples of cell bodies were displayed in panes of Figures 5-15.

2.a. NN thalamus:

NN neuron cell bodies were typically oblong to round shaped according to randomness of sectioning. They contained a large euchromatic nucleus with minor to deep indentations that gave them with LM semi-thin sections a sort of wrinkled coffee bean-like aspects. Their heterochromatin content was faintly dispersed throughout the nucleoplasm as discrete clusters while a few rare packets decorated the inner nuclear envelope membrane with a part that constituted the chromatin associated portion of the nucleolus. The nucleolus often reached 1.5 to 3.5 µm wide and displayed characteristics of a very active cell. There, the chromatin associated (CA) with the nucleolus component was noticed as the most heavily contrasted component of the active nucleolus forming wavy, dense entwined swirls (dense fibrillar region or DF) delimitating circular zones containing the fine fibrillar regions (or FF), altogether named nucleolar organizer centers or NORs. Thus, a NOR usually appeared as a round hole perforation-like of the netting aspect whose content usually is a fine fibrillar region or body where the ongoing transcriptions occurred (Figs 5 A-D and 6), as recognized and identified by previous studies. An enormous nucleolus with numerous NORs is depicted in Figure 5 C-D where the resulting transcripts can be recognized as innumerable ribonucleoproteins and appeared as accumulated granular component. According to activity of the cell, these accumulations, within the meshwork of DF can create an overflow granular 'cloud' that constituted the other nucleolus component or granular center (GC) of the nucleolus within the nucleoplasm (Fig 5D). Again, any random sectioning plane sometime did not allow to view the entire complexity of the nucleolus. In any favorable case of plane of ultrathin

sectioning, the neuron nucleolus was most often detected in a subcentral core position of the nucleoplasm associated with a zone where one deep indentation of the nuclear envelope existed as seen with LM views (Figs 3, 4 and 5 A-D). The perikaryal areas of the neuron cell bodies seemed narrow but crowded by typical cell's organelles such as small stacks of Nissl bodies where RER-SER and free polysomes accompanied concentrically-located saccular packets of Golgi apparatus, small but numerous mitochondria and a few lysosomal bodies among which some displayed pale inner fatty droplets, making them typical lipofuscin residual deposits. It necessitated some scrutiny to detect some of the axo-somatic synaptic zones along the perikaryal neurolemma as marked with arrows (Fig 6).

2.b. HN thalamus:

At first glimpse, this chronic hyponatremia treatment featured HN neurons that displayed a serrated or crumpled to round aspect, according to their location that went along with a matching pattern of the nucleus shape (Fig 7 A-B). A rounder aspect can be noted when adjacent to blood vessels (Fig 7A) while the elongated, crumpled shape, was noted in the neuropil (Fig 7 B). In all cases, the large euchromatic nucleus reminded the large NN ones while the astrocytes or oligodendrocytes contrast was changed, as highly enhanced compared with those NN ones, as suggested by semi-thin sections (Fig 3 HN) as also noted in other studies by [72-74]. Furthermore, the nucleus envelope wrinkled outline was enhanced by the small accumulated blotches of heterochromatin (0.1 to 0.8 µm long) along the inner membrane while accumulated 35-150 nm specks or knots of heterochromatin distributed throughout the nucleoplasm. In some areas of this nucleoplasm, groupings of 35-65 nm wide specks were seen in the loosen marble-like, entwined small heterochromatin condensations. In these HN cells, a densely contrasted nucleolus was disclosed demonstrating a dissociation into its subcomponents, especially between the compacted ribonucleoproteins viewed as round to piriform granular center (GC), its discrete nucleolemma interstices and its associated heterochromatin (CA) outlined by a progressing rift between the GC mass and the CA components (Figures 7 A-B and D). Other features of neuron cell bodies were the perikaryon organelles such as winding saccules of endoplasmic reticulum (ER) showed contrast but were free of the disseminated, surrounded polyribosome strings and a major Golgi zone. Other membranous structures appeared as lysosomal bodies or autophagosomes insulating damaged structures, forming wraps and contained some polysomes. Several peculiar round aggregates, dense to electron, and ranging from 100 to 250 nm in width, decorated the neuroplasm and emerged in the adjacent neuroplasm of these Golgi cisterns. These bodies occurred without a limiting membrane and made of hazy material that even after scrutiny of a higher ultrastructural magnification did not resolve into any structured organelle or cytoskeletal microfilaments (Fig 7 C). This hyponatremia seemed to have induce minor cristae swelling of

the many but small mitochondria found that did not display evident gross swelling and hypertrophy like those of macroglial cells.

2.c. ODS12h thalamus:

c1. Inside the zone of degraded myelin:

If degradations of the neuropil at ODS12h were nor visible with LM, TEM observations were able to detect early significant defects that occurred within the worst damaged areas only viewed with LM at ODS48h, i.e. the nerve cell bodies were mainly preserved during these ongoing demyelination injuries involving the distal cell extensions and the macroglia (Fig 8 A-E). These neurons usually displayed a compact, sub centrally-located nucleolus that showed complete dissociation between its components involved in transcriptional activities, i.e. the chromatin associated with the nucleolus was segregated away from the granular center that formed a sphere-shaped mass speckled by tiny pale-contrasted regions, maybe as left-overs or constricted fine fibrillar centers. The amassed macromolecular structures revealed fine, sprinkled dot pattern of 20 nm or less in size; additionally, no evident nucleus envelope indent was found (Fig 8 A, B and D). Most of the time, the perikaryon adjacent to the nuclear envelope revealed in all neurons one long curved emptied vacuolated space amongst the neuroplasm and amongst grossly swollen mitochondria, endoplasmic reticulum (ER) cisterns and lipofuscin bodies that contrasted with accumulated small size, disintegrated-like polysomes. There, parts of were noted with disintegrated Golgi zones. Membrane seemed to have incurred 'fragilization' because showed single leaflet membrane as unilateral remnants as curve-shaped and teared areas of the neuroplasm that cannot be identified as parts of that ER (Fig. 8 A-E). If some initial segment as axon hillocks can be seen (e, g, Fig. 8 A), other structures, such as axo-somatic synapses, noted in NN cells, were not recognized.

c 2. In the adjacent reactive astrogliosis zones, at ODS12h:

Further away from the deteriorated region, ODS12h neurons preserved cell bodies with axon hillock extensions, even if some were difficult to outline (Fig 9 A-D). However, most ODS12h cell bodies maintained axo-somatic synaptic zones along the neurolemmal perimeter as exemplified in Figure 9 D. The nerve cell bodies were still the largest cells amongst the neuropil showing round to ovoid nuclei appeared euchromatic and kept only small indents while the nucleoli condensed in large accumulated-like and elongated complex spheroids of granular ribonucleoproteins that seemed separated by narrow splits from the associated contrasted, chromatin fibrillar region aggregated, detected as one or more neighbouring patches. Most of these features revealed stoppage of transcriptional activities but not enduring damages found in oligodendrocytes and astrocytes. Simultaneously, a loosen, marbled aspect of the nucleoplasm exposed its euchromatic features with displays of innumerable freckles of

heterochromatin whose groupings can be revealed throughout the nucleoplasm and outwardly enhanced the inner membrane of the envelope. The perikaryon also contained a few erratically long, winded RER cisterns accompanied by lots of small polyribosomes where several small stacks or elongated Golgi apparatus saccules were viewed as circumscribing dilated parts of the perikaryon. In the same areas, the surrounding neuropil contained parts of intermingled oligodendrocytes (Fig 9 B and D), conspicuous with their condensed nucleus and cytoplasm, indicating that general acidification and distal, regional damages these cells had undergone while ODS recovery was apparently happened in neurons, as seen in this study. These nerve cell bodies were noted having preserved many axosomatic synaptic zones (Fig. 9 D).

3. ODS48 h thalamus:

As a result of this treatment, neuron cell deaths were never found whether with LM or TEM. Instead, in the adjacent neuropil of these neuron cell bodies, ODS demyelination damages lingered as swollen vacuolated corpses of axons and voids, displaying variable widths, were further evidences of degradations (Fig. 10 A-C). ODS 48h neuron cell bodies demonstrated large size. In these cell bodies, the nucleoli became again constituted by a highly contrasted, thick fibrillar component (or chromatin associated) that formed small were noticed as evidences of huge transcription activities with only small granular adjacent regions (Figs 11-13). heightened and sometimes branching nuclear envelope furrows and with some of them appeared reaching inwards and abutted the nucleolar structure (Figs 11-13). Most nucleoli rebuilt up their entwined components and became as large as 5-7 µm long (Figs 11-A-E, 12A-B, 13 A-D). There. NORs were again easily detected as accentuated twirls or tight chromatin spirals wherein narrow poor contrasted, fine fibrillar regions developed and both got surrounded by clouds of granular centers of huge number of ribonucleoproteins (Figs 11 -13). At this time course of thalamic experiment, perikaryal translational activities were also adjusted by the functional organelles similar to those typified in NN neurons: polyribosomes and some RER, Golgi apparatus with stacks of saccules, small and elongated mitochondria and neurotubules even though Nissl bodies were not evident amongst the innumerable ribosomes, in dispersed forms either as free polysomes or attached to the endoplasm saccules. Many lysosomal bodies as remnants of autophagosomes and lipofuscin bodies can be viewed, along the nuclear envelope left and, in some cells, fragile tiny zones (Fig 10 A-C) or amongst the wide perikaryal other organelles (Figs 14 and 15). There neurotubules are haphazardly scattered among neuroplasm fields. In some neurons, recovering axo-somatic contacts and the many perikaryal functional organelles revealed peculiar fibro-granular aggregates that can reach 1-1.5 µm in diameter, such as in Figure 11A, enlarged in Figures 14 and 15. A scrutiny of them showed protuberant filamentous and granular components. There, the granular components seemed to reach the size of ribosome particles or parts of them while the

intermingled thin filaments reached much less than 7 nm and are closely matched with either some mRNA inter-ribonucleoproteins or as actin cytoskeleton, unless tangled oligomer parts of neurofibrils but those could not be detected in these damaged zones under reactivation but in other cortex zones, adjacent to thalamus [73]. Meanwhile, we have reported [72-74] that, satellite oligodendrocytes (Fig. 13 A and C) and interfascicular ones as well as astrocytes, after enduring reactive astrogliosis - as clasmatodendrosis – survived after damages and were recognized by their loose deposits of beta-glycogen particles (Fig 14, as in [74]. In this study, they were again detected, not without scrutiny, among the neuropil as delicate extensions by resolving spread of the same beta-glycogen particles in most sections of the specimen studied, but only with the highest magnifications.

Discussion

Neurons cell bodies have been reviewed extensively in classic textbooks dealing with normal ultrastructure and some pathology [83-88]. There, most features described and reviewed with fine structure aspects belonged to the CNS pyramidal and cerebellar structures while myelination formation, biochemistry and as well as and defects were also parts of more specialized books [89-90] but very few of them have dealt with thalamus fine structure [85, 91-94]. However, thalamus connectivity has been done in scarce publications (i.e. [95]) and some authors who have even entitled 'ultrastructure' in their reports only illustrated with light microscopy (i.e. 54, 94, 96) while others showed morpho-functional interconnections [97-100].

1. ODS Demyelination in the murine thalamus:

The thalamic neurons studied are part of the relay ventral posterolateral (VPL) and ventral posteromedial (VPM) nuclei [85, 91-92]. These thalamic osmotically extrapontine-susceptible regions contain neuroglial cells that undergo injuries and cell deaths recognized to incur as regional damages associated with myelinolysis [72-74, 101-103]. These regions are essentially constituted by inhibitory interneurons that synthetize GABA or neuropeptides as neurotransmitters [104] and modulated by numerous serotoninergic or norepinephrinergic axons interrelationships can see their functions altered by ODS [72]. If nowadays, ODS clinical defect is now being adjusted [105], literature still contains clinical cases developed along a similar neuropathologic pattern which outcome has still need to be best cared for by understanding the etiology and defect outcome [106-108], probably originating from astrocyte signals caused by the osmotic stress [73- 74, 101-103] and defect in the blood-brain barrier [111-112]. In the CNS, thalamus is a region where most frequent ODS myelin loss first occurred; it has one of the highest energetic demands of the CNS, confirmed by

tomographic imaging for its peculiar sensitivity [113], maybe implicating some neurovascular coupling [114-115].

Thalamic neurons have been described in some aspects of morphology encompassing the relay functions deemed by these areas of the thalamus, but only a few studies included ultrastructure aspects in mammals [91-93, 116- 123]. In other studies, where a rapid correction of chronic hyponatremia in rats recapitulates most of the human ODS histopathology, it was shown that myelin and oligodendrocyte losses occurred with neurons and axons sparing in specific brain regions such as cortical regions, hippocampus and basal ganglia associated with somatosensory relationship defects [64,101-102]. In this paradigm, following other similar studies [72-74], the same murine model developed an astrocytopathy leading into oligodendrocytopathy with unambiguous demyelinating lesions in the thalamus, as shown in Figure 2 A-D. Following haematoxylin and eriochrome cyanine R staining, parasagittal brain sections demonstrated a conspicuous loss of myelin of the white matter in several specific regions, such as the thalamus, colliculus, and pons. The demyelinated thalamus region was delimited with sharp borders in ODS48h brains but no obvious difference of myelin staining was observed between NN, HN and ODS12h thalami (Figure 3 A-C). The ventral posterolateral (VPL) and ventral posteromedial (VPM) nuclei examined with other immunomarkers for myelin (i.e. myelin basic protein or MBP) confirmed myelin loss in the same areas and quantitative changes of this immunolabelling showed a clear myelin loss at ODS 48h and at later time points [72-73]. There, an exhaustive list of demyelinated brain regions, such as thalamic nuclei, parietal associative cortex, secondary visual cortex, primary motor and somatosensory cortex were the most damaged and again data were comforted by combined imaging and energetic data by Hochstrasser and collaborators [113]. Demyelination was never detected in highly myelinated tracts (i.e. the corpus callosum or the anterior commissure).

2. ODS and NeuN labelling:

Subtle differences in the immunolabel density can be noted amongst treatment groups but, taking account that each microscopic preparation was batch-processed similarly, these differences could likely relate with the dynamic variations of the changed nerve cell functions associated with the expression of nuclear and cytoplasmic transcript proteome. NeuN immunolabeling have been discussed by several authors and it has been verified to specifically and exclusively mark the mature neuron nucleus [124-127] and in its altered states, including neuro-oncology [128-130]. The same studies never found NeuN labels in immature neural progenitor cells nor macroglial cells. Some authors have also noted a decreased immunostaining could be elicited by a temporary suspended synthesis of some neuron proteins due to damage while viability was preserved, e.g. histone proline component

(Williamson, 1994). When using a moderate ischemia model (30 min ischemia), it was found that neurons lose NeuN immunoreactivity 6 h after exposure, while retaining the integrity of the NeuN protein. This product of the Fox-3 gene (Fox abbreviated for 'Feminizing locus on X' with 3 types of genes 1, 2 and 3) belongs to the Fox-1 gene family of splicing factors, including synapsin I [131-133]. Fox-3 was essentially located in the nuclear matrix and, thus, marked only mature neurons for heterogeneous ribonucleoproteins or hnRNPs [134-135] also located in the nucleoplasm and detected through Western blots that disappeared with RNase A treatment; a constant SRm160 and constant translocation shuttling between neuroplasm and perikaryon transcripts toward perikaryons as a follow up from Fox-3 activities [127,136-138].

Thus, in NN, HN and ODS48h experiment groups, alternative splicing likely regulated and modulated many of the thalamic neuron proteins through spliceosome's processing and affected transcriptional RNAs along the fine fibrillar center inner edges of the nucleoli [139-150]. This label pattern would agree with studies where NeuN label cross-reacted with the production and turnover of synapsin I, traced in the cytoplasm (e.g. [131,151]). One could assume that, in Figure 3 ODS12h, the cell bodies featured a poor labelled NeuN nucleoplasm also reflected a stoppage or depleted transcriptional activities while some labelled products were already in the neuroplasm, i.e. this staining pattern may locate NeuN isoforms preserved by fixation process as shuttling components or factors exchanged between nucleus and neuroplasm. Therefore, the sorting of the adequate synthetic macromolecular proteome maintained in NN neuron's functions, e.g. receptors, ion channels, including aquaporins, tau proteins, aspects of neural plasticity dealing with presynaptic components [127, 131, 137-138,152-154] has been reactivated as NeuN indicated from weak nucleoplasm ODS12h contrasted pattern toward a stronger nucleoplasm label in the nerve cell bodies of the ODS48h treatment.

3. ODS LM semi-thin sections as morphologic clues:

LM views of µm thick epoxy sections of all the treatments showed morphology changes of the nuclei, from oblong to round and indented with large contrasted nucleoli in a sort of sequence: NN = ODS48h > ODS12h > HN, where HN cell bodies and nuclei displayed shrivelled aspects. LM features did not reveal changes in the neuroplasm but, between treatments, the surrounding neuropil displayed interstitial gaps more abundant in ODS48h than in ODS12h samples as many large voids probably resulted from the demyelinating damages, likely comforting the microgliocytes activity, removing corpses as debris of some oligodendrocytes, astrocytes and parts of demyelinated axons throughout the affected zones [72-73]. The epoxy semi-thin sections can again comfort the histology detection of thalamus damages observed

in LM paraffin views as in Figure 2 and other brain sections viewed of the same experimental experiment [73].

4. ODS TEM morphologic features:

In this murine ODS model, content and topologic changes of neurons, macroglia (astrocytes and oligodendrocytes) and microgliocytes have been verified, including those of cytoskeletal expression disturbances, with immunolabels. There, some of the fine structure investigations of macroglia, microglia and of the neuron cell bodies of the same murine thalamus regions that underwent the same ODS conditions have been swiftly perused [72-73] and have been further supplemented in this fine structure analyses by focusing on the nucleus content and some perikaryon contents of the nerve cell bodies. The cell bodies of the ODS48h group most resembled the NN or Sham group, and thus, encouraged this further fine structure scrutiny, as reported, after comparisons made with the HN and ODS12h cohorts, in continuation with these previous studies on the ODS murine thalamus.

4.a. The neuron nucleus morphology

The typical functional morphology of the thalamus region studied contained NN or Sham nuclei revealed by their invaginated envelopes where many notches depths observed depended on the random plane of sectioning whose shapes are probably influenced by the cytoplasm/neuroplasm matrix modifications that accompanied changes in translational activities and of the extracellular environment changes, as verified in vitro and in vivo by others both in relationship with interphasic activities [155-168]. The changes associated with hyponatremia displaying cell and nucleus outline's perimeter wrinkled and content revealed the combination of osmotic shock and changes the supportive cytoskeleton ensued with processing of the tissues [158-159, 170-173]. The same changes went along with the detection of small, round mitochondria profiles with loss of cristae and only discrete swelling changes in the ER that also lost most attached ribosomes and polysomes, contrarily to the more evident observations made with the macroglia - astrocytes and oligodendrocytes- in hyponatremia where mitochondria revealed evident alterations, such as swelling and hypertrophy [72-73; 111-112]. The lowest magnification of the electron microscope made us to compare at least 20 cell bodies from each treatment group; this qualitative survey indicated the nucleus shapes varies from round to oblong or oval with notches and with large, compacted nucleolus in the following sequence: NN = ODS48h > ODS12h > HN. Noting the similar finding as with the LM views of 1-µm thick epoxy sections.

There, the cell's nucleus and, especially, the nucleolus components, demonstrated changes in component's assembly revealed active (NN cells) to inactive (HN cells and ODS12h) and back to operating activities (ODS48h) i.e. where the accumulated mass of GC or

ribonucleoproteins are not delivered in the perikaryon, i.e. they formed a huge transcript mass blocking further new transcripts, similarly to other models of post-injury of neural plasticity [139-150, 174]. Bearing in mind that the nucleolus, now known as a contrasted body 'inclusion' of the 'organelle' nucleus of the cell was discovered more than 180 years ago [175-177] is significative that at LM level, tissue degradations were detected in regards with those of macroglial components of the CNS, but ultrastructure verified that, 48h after rebalancing osmolarity, suggestive aspects demonstrated the restoration of neuron nucleus and nucleolus functions have already happened.

4.b. The neuron cell body and nucleolus fine structure changes

ODS12h neurons compared with the HN neurons had an oblong to oval-like nucleus and the nucleus not only became rounder than the HN one but also small indents managed to appear, reacquiring a sort of functional morphology of neurons with a still somewhat compacted nucleolus and heterochromatin packs layered along the inner envelope. These chromatin modifications have been already described as 'clumping' in the rat ODS [111-112].

In the myelinolytic areas, where the neuron cell bodies remained with a Wallerian-degeneration type, changes not detected with LM in both the nucleus and perikaryon can be discriminated by ultrastructure where most interesting changes occurred in the nucleolus. The nucleolus components in ODS12h neurons closely surrounding of the worst myelinolysis showed segregation but to a lesser extent than the central, core damaged zone, dismantled and the accumulated granular components transcripts separated away from the core nucleolus, loosing NORs, a pattern signified either a poor to obliteration or transient latency in making transcripts of the treated cells. This nucleolus changes had received a large body of evidences either in cell and molecular experiments, documented by numerous authors dealing with normal or treated cancer cells**,** revealing ultrastructure that complemented those of the earliest morphologists that identified and investigated several specific ultrastructural immuno-molecular markers [139-150, 178-208] and in monographs and books on the topic [i.e. 142, 158, 164, 183, 207-209]. During these injurious-like and peculiar self-salvaged conditions (ODS12h to ODS48h), the energetically-demanding transcriptional and translational activities needed to be largely forfeited for some minimal glycolytic maintenance [204, 206-215] in order to preserve the nucleus and genome makeup during this period hyponatremia and immediately post hyponatremia, i.e. ODS while enduring a recuperation of osmolality. This type of safeguard has been noted in the thalamus ultrastructure has been also supported in another study [216]. Although, astrocytes usually maintained most energetic demands of neurons, as noted by persisted beta glycogen particles in ODS [217-220]. In ODS like other cytotoxic cell conditions of the normal or stressed tumor cells,

neurons could adapt or upheld a minimal functioning for their sake and assumed for a time, glycolysis [221-222] within the same time-frame (i.e. ODS12h period), clasmatodendrosis has been found. This astrogliosis encompassed self-excisions of cell pieces and oligodendrocytes lost maintenance of myelin [73-74]. One may assume also that some uptake of intercellular, diffused metabolites (i.e. amino-acids) could be done [222] and that some typical routes, via remained adjacent oligodendrocytes and astrocytes, left unaffected by ODS in the same murine model, reached the resilient neuron cell bodies [72-74] because, the dependence of traumatized neurons on glycolysis and oxidative phosphorylation remained unclear [222].

At ODS 48h, the chosen time lapse after osmolarity was rebalanced was marked by a return of apparent functions for the thalamus region investigated. All ODS 48h neuron cell bodies (as shown in Figures 11 D, 12 A-B and 13 A-C), the nuclear envelope indents equipped the euchromatic cells with increased surfaces of delivery between nucleus products and the neuroplasm, perikaryon, adjacent and likely repair transcripts to get into translational activity. The processed transcripts emanating out of the nucleolus reached the neurolemma surfaces enlarged, perikaryon gorges to disperse in the perikaryon and away using some sorts unmarked alleyways or tracks within the nucleoplasm. A general morphology comforted the nuclei that have restored functions similar to those of the Sham control or NN cell bodies of the same CNS region because even if the nucleus does not change volume from round to elongated ovoid, they revealed homeomorph topologies by increased notches or indentations of their envelope section's profiles. In addition, the reappearance of the nucleolus NORs, where heterochromatin associated with the nucleolus developed dense fibrillar component, and out of it, fine fibrillar regions (chromatin unpacked from histones where transcripts are formed in the small, circular greyish areas) where alternative splicing occurred and still not clearly understood for its roles in neuronal biology. There spliceosomes must assemble onto each intron to catalyse its excision, and this assembly is controlled by a large number of pre-mRNA-binding proteins. These coincidental aspects of active restoration of the central machinery provided in normal and alternative splicing transcripts along with translational capabilities abundantly verified by ribosome, polyribosomes, processing ones [223] and the organelles found in the ODS48h [224, 139-150, 224]. **T**he outer nuclear leaflet being an extension of the RER [171, 225-233]. The processed ribonucleoprotein precursors, accumulated in the nucleoplasm then translational macromolecules reached the perikaryon, through the nucleus envelope increased surface and allowed for more nucleoplasm-neuroplasm exchanges in providing more nuclear pore passageways for transcripts at sites for homeostatic maintenance and functional cell's activities verified by some reestablishment of typical neuroplasm structure notably, the polysomes, rough ER and Golgi apparatus appearances. The ODS 48h narrow, immediate concentric perinuclear neuroplasm with

essential cell structures maintained then seemed to refurbish by restitution of the perikaryon organelles. Thus, the nucleolus of the nucleus of the neuron cell bodies revealed NORs, large amounts of perikaryal polyribosomes revealed the re-established nuclear transcription activities have a pathway to translational ones because of the complete reorganization and rehabilitation of perikaryal organelles, such as RER, Golgi apparatus saccules, even though the distal extensions and interconnected neuropil components were still with defective structures. In some areas, peculiar 'nail-cut shaped teared areas of the neuroplasm were found, either indicating some cytoskeletal disturbances or fragile neo-formed phospholipid structures.

4.c. The neuron cell body and the organelles

Two days after osmolarity was rebalanced, the Wallerian, pruning demyelination zone [234. [234-237] that can take a few days (e.g. 2-3 days) in rats [238] had finally provoked -at this ODS 48h time lapse - frothy aspects of many places of the neuropil as seen again in [72-73]. where accretion of intercellular or neuropil remnants of injuries were found throughout the ODS regions, with variable degree of vacuolated-like aspects, resolved as small voids or spaces located in the interstitial neuropil myelinolysis around the withstanding cell bodies; there were no inflammatory response (as seen in Fig. 4 ODS48h). There have been removal of debris or corpses that succeeded (after clasmatodendrosis [72-74]) because microglial cells changed morphology without other course than containing phagosomes [72-73] while neuron cell bodies were still preserved in the same demyelinated areas, contrarily to that reported in [239]. Some salvage strategies, avoiding cell trauma towards neuron cell death seemed similar to [240]. The definition of ODS remained [72-73] because the main degradations occurred, caused by a disrupted osmotic gradient initiated in the vascular supply, transmitted injurious change signals to astrocytes that expanded into submitting oligodendrocytes into inadequate maintenance of the myelin [74, 89] allowing some prompt but short-timed implication of the microgliocytes, properly 'trained' to then remove defective parts without creation of any other immunoreactive nerve tissue defects like in multiple sclerosis [113, 241] as defined by the ODS condition [64-66, 72-74, 235] but where clarifications are still needed [242]. At ODS 48h, myelin sheets have not all recovered and those repaired still contained disordered concentric layers due to intermembranous gaps and delicate smudge-like aspects. In the core of degradative zones, intercellular spaces created by removal of axonal debris or corpses created free spaces within the surroundings of the neuron cell bodies, corresponding at fine structure level of what is called in classic histopathology terminology the spaces that resulted of necrotic CNS tissue as 'liquefaction necrosis' [243-245].

4.d. The perikaryon and peculiar fibro-granular bodies:

Concurrently or associated with the tissue restorations that have been able to be shown with the astrocytes [72-73] one can verify that, the neurons of the thalamus, altered from myelinolysis as a result of ODS, after fixation and processing, some re-establishment and dispersion of transcripts toward a huge output in the neuroplasm of the thalamic cell body regions examined, revealed rare but peculiar accumulated structures in the form of fibro-granular aggregates or bodies, somewhat noted in some astrocytes at the same ODS 48h time-point [73-74]. In these regions of the thalamus, neuronal inclusions have been found [246-248]. However, they are not made with membranes, thus cannot be considered as bunina bodies as shown in reconstructed neurons [249] and they were not degenerating or associated with endosome or lysosomes [250]. These structures, made of entwined and coiled fine filaments, are mixed with adherent granules smaller than ribosome granules but measured up their subunit size [252-258]. The filamentous network that appeared outwardly of these structures were very thin macromolecules (less than 5 nm in diam.) and could be of cytoskeletal actin and/or of associated depolymerized proteinaceous structure(s) linked with the ongoing dispatching or trafficking of ribonucleoprotein transcripts [257-259] as they associated with the nuclear creases accumulated while some proteome repression occurred [259] as in the case of the S100 protein in PNS? [260]. Alternatively, if one considers that a functional nucleus undergoes oscillating waves, huge amounts of transcripts disseminated in the surrounded restoration neuroplasm to be proteome/metabolome translations and, associated with transport cytoskeleton 'sudden' loads of ribonucleoproteins[260-265] with the nucleus topology changed (indents as spheroid), immersed in a viscous liquid flow, could act as sort of swinging watermill surrounded by those cytoskeletal macromolecules, mainly actin [172, 173, 260]. This oscillating, turbulent flow in the neuroplasm could induce one eddy at the opposite side of the axon hillock along with the less mobile, concentric organelles [266-267]. These mechanic stagnation points in the perikaryon layer would then provoke a deposition or pile up of collected translational materials for proteomes alongside cytoskeletal and/or supportive macromolecules [257, 268-271]. Post ODS, oligodendrocytes seemed to recover much later than the period studied here because the typical markers used for myelin expression showed with LM 'demyelinated' zone in Figure 2 ODS48h and [72-73] while electron microscopy data reviewed here suggested that healing processes encompassed the same thalamus nuclei, where intracellular phase separation dynamics would reorganize the perikaryon components [272-273] and new data revealed axon hillock and myelination recovery through reconstructed microtubule markers (not shown here and to be submitted), probably alike most favorable human neurologic healing post-ODS..

Conclusion

Delay in Wallerian degeneration in CNS in comparison to PNS and, probably in regeneration as well, is not due to a delay in axonal degeneration, but rather is due to the difference in clearance rates of myelin between CNS and PNS [234, 238]. In this report, the murine thalamus nuclei fine structure aspects can bring some new, interesting aspects relevant to other future murine neuropathology studies, especially those that would later involve knock out models and relate to ODS human situations where demyelinating defects encompass traumatic origin that associated with metabolic depletion of [Na+] (and other osmolytes) whose homeostatic restoration induced repairs [274]. This model can indicate that only ultrastructure would verify the changes endured by resilient neuron cell body nucleus and perikaryon out of a short-term Wallerian defect through some adaptative cell metabolic strategies. One could also speculate that adjacent external zones of the damaged deteriorating regions with a blood-brain barrier remaining intact would assist with the less damaged and maintained astrocytes intercellular contacts with neurons and would facilitate in the structural and some functional resistance and reconstruction [64, 71-74, 101-103, 111-112]. In ODS, no blood born cells or proteins have been spilled out like in other neurodegenerative defects (i.e. multiple sclerosis or other CNS vascular trauma associated pathologies) making the injurious region damaged free from other immune reactivity [114, 115, 135, 275] and other eventual potent follow-up necrotic neural sequels [276, 277]. In ODS, clinical controlled rebalancing sodic osmolality allowed rapid neuron reactivation of their functions that involved, among others, aquaporins [109, 278-280].

Experiments that included molecular markers and ultrastructural verifications obviously can further verify and achieve clarifications of the cellular components involved in the regenerative plasticity of this type of mammal and human CNS damage where some data have only been scarce before the advent of recent molecular tools [103, 110]. Here, the report demonstrates that the fine structure morphology of the nucleus alone and nucleolus content, as referred abundantly above, as in [281], can assist to diagnose and understand whether neuron repairs occur in the animal models of neuropathology tested to eventually be translated into potential clinical outcome for some patients who developed defects post ODS [27, 282-283].

Literature Cited

1. Adams, V, Mancall EL. Osmotic demyelination syndrome. Am J Med Sci 1959; 339 (6): 561-567.

2. Newell KL, Kleinschmidt-Demasters BK. Central pontine myelinolysis autopsy: a twelve-year retrospective analysis. J Neurol Sci 1996; 142:134- 139.

3. Martin RJ. Central pontine and extrapontine myelinolysis: the osmotic demyelination syndromes. J Neurol Neurosurg Psychiatry 2004; 75 (suppl 3): iii 22-iii28.

4 Abbott R, Silber E, Felber J, Ekpo E. Osmotic demyelination syndrome. BMJ 2005; 331 (7520): 829-830.

5. Tullu MS, Deshmukh I, Muranjan MN, Kher AS, Lahiri KR. Extrapontine myelinolysis in a child with nephrotic syndrome. Pediatr Neurol 2010; 43(2):139-141.

6. Zhu RJ, Lu ZS, Shan CL, Xu MW, Luo BY. Pure word deafness associated with extrapontine myelinolysis. J Zhejiang Univ Sc B. 2010; 11 (11): 842-847; doi: 10.1631/jzus.B1000200.

7. Alleman AM. Osmotic demyelination syndrome: central pontine myelinolysis and extrapontine myelinolysis. Semin Ultrasound CT MR. 2014; 35(2):153-159.

8. Singh T.D. Fugate J.E. Rabinstein AA. Central pontine and extrapontine myelinolysis: a systematic review, Eur J Neurol.2014; 21 (12): 1443–1450.

9. Laureno R, Karp BI. Myelinolysis after correction of hyponatremia. Ann Intern Med.1997; 126(1):57-62.

10. Babanrao SA, Prahladan A, Kalidos K, Ramachandran K. Osmotic myelinolysis: Does extrapontine myelinolysis precede central pontine myelinolysis? Report of two cases and review of literature. Indian J Radiol Imaging. 2015; 25:177–183.

11. Laureno R, Lamotte G, Mark AS. Sequential MRI in pontine and extrapontine myelinolysis following rapid correction of hyponatremia. BMC Res Notes. 2018; 11(1):707. doi: 10.1186/s13104-018-3816-5.

12. Gocht A, Colmant HJ. Central pontine and extrapontine myelinolysis: a report of 58 cases. Clin Neuropathol. 1987; 6(6): 262-270.

13. Brunner JE, Redmond JM, Haggar AM, Kruger DF, Elias SB. Central pontine myelinolysis and pontine lesions after rapid correction of hyponatremia: a prospective magnetic resonance imaging study. Ann Neurol.1990; 27(1): 61-66.

14. Kimura K, Yasaka M, Terasaki S, Oita J, Yamaguchi T. [A case of central pontine and extra-pontine myelinolysis demonstrated by magnetic resonance imaging]. [Article in Japanese] Rinsho Shinkeigaku.1991; 31(11):1202-1207.

15. Yuh WT, Simonson TM, D'Alessandro MP, Smith KS, Hunsicker LG. Temporal changes of MR findings in central pontine myelinolysis. AJNR Am J Neuroradiol.1995; 16:975–7.

16. Cramer SC, Stegbauer KC, Schneider A, Mukai J et al. Decreased diffusion in central pontine myelinolysis. AJNR Am J Neuroradiol. 2001; 22(8):1476-1479.

17. Ruzek KA, Campeau NG, Miller GM. Early diagnosis of central pontine myelinolysis with diffusion-weighted imaging. AJNR Am J Neuroradiol.2004; 25(2):210-213.

18. Hagiwara K, Okada Y, Shida N, Yamashita Y. Extensive central and extrapontine myelinolysis in a case of chronic alcoholism without hyponatremia: a case report with analysis of serial MR findings. Intern Med. 2008; 47(5): 431- 435.

19. Dujmović I, Vitas J, Zlatarić N, Drulović J. Central pontine myelinolysis in a chronic alcoholic: A clinical and brain magnetic resonance imaging follow-up. Vojnosanit Pregl. 2013; 70: 785–788.

20. Bhatia S, Kapoor AK, Sharma A, Gupta R, Kataria S. Cerebral encephalopathy with extrapontine myelinolysis in a case of postpartum hypernatremia. Indian J Radiol Imaging.2014; 24: 57–60.

21. Zunga PM, Farooq O, Dar MI, Dar IH, Rashid S, et al. Extra pontine osmotic demyelination syndrome. Ann Neurosci. 2015; 22: 51–53.

22. Barhaghi K, Molchanova-Cook O, Rosenburg M, Deal B, et al. Osmotic Demyelination syndrome revisited: Review with neuroimaging. J La State Med Soc.2017; 169(4):89-93.

23. Garg P, Aggarwal A, Malhotra R, Dhall S. Osmotic demyelination syndrome - evolution of extrapontine before pontine myelinolysis on magnetic resonance imaging. J Neurosci Rural Pract. 2019; 10(1):126 -135.

24. Adrogué HJ, Madias NE. Hyponatraemia. N Engl J Med. 2000; 342 (21): 1581-1589.

25. King JD, Rosner MH. Osmotic demyelination syndrome. Am J Med Sci. 2010; 339(6):561-567.

26 Aratani S, Hara M, Nagahama M, Taki F, et al. A low initial serum sodium level is associated with an increased risk of overcorrection in patients with chronic profound hyponatremia: a retrospective cohort analysis. BMC Nephrol.2017; 18(1):316. doi: 10.1186/s12882-017-0732-1.

27. George JC, Zafar W, Bucaloiu ID, Chang AR. Risk factors and outcomes of rapid correction of severe hyponatremia. Clin J Am Soc Nephrol. 2018; 13(7):984-992.

28. Woodfine JD, van Walraven C. Criteria for hyponatremic overcorrection: systematic review and cohort study of emergently ill patients. J Gen Intern Med. 2020; 35(1):315-321.

29. Crismale JF, Meliambro KA, DeMaria S Jr, Bronster DB et al. Prevention of the osmotic demyelination syndrome after liver transplantation: a multidisciplinary perspective. Am J Transplant. 2017; 17(10): 2537-2545.

29. Filippatos TD, Makri A, Elisaf MS, Liamis G. Hyponatremia in the elderly: challenges and solutions. Clin Interv Aging. 2017; 12: 1957-1965. doi: 10.2147/CIA.S138535.

30. Aegisdottir H, Cooray C, Wirdefeldt K, Piehl F, Sveinsson O. Incidence of osmotic demyelination syndrome in Sweden: A nationwide study. Acta Neurol Scand. 2019; 140(5):342-349.

31. Adams RD, Victor M, Mancall EL. Central pontine myelinosis: a hitherto undescribed disease occurring in alcoholic and malnourished patients. Arch Neurol Psychiatry. 1959; 81 (2):154- 172.

32. Mascalchi M, Cincotta M, Piazzini M. Case report: MRI demonstration of pontine and thalamic myelinolysis in a normonatremic alcoholic. Clin Radiol. 1993; 47:137–138.
33. Kelly J, Wassif W, Mitchard J, Gardner WN. Severe hyponatraemia secondary to beer potomania complicated by central pontine myelinolysis. Int J Clin Pract. 1998; 52:585–587.
34. Liamis GL, Milionis HJ, Rizos EC, Siamopoulos KC et al. Mechanisms of hyponatraemia in alcohol patients. Alcohol. 2000; 35:612-622.
35. Mochizuki H, Masaki T, Miyakawa T, Nakane J, et al. Benign type of central pontine myelinolysis in alcoholism – clinical, neuroradiological and electrophysiological findings. J Neurol. 2003; 250: 1077–1083.
36. Uchino A, Yuzuriha T, Murakami M, Endoh K, et al. Magnetic resonance imaging of sequelae of central pontine myelinosis in chronic alcohol abusers. Neuroradiology. 2003; 45: 877-880.
37. Kuhn J, Harzheim A, Bewermeyer H. [Central pontine myelinolysis with a hyperintense lesion in diffusion weighted MRI: overview by means of a case report]. [Article in German]. Röntgenpraxis.2005; 56(1):21-27.
38. An JY, Park SK, Han SR, Song IU. Central pontine and extrapontine myelinolysis that developed during alcohol withdrawal, without hyponatremia, in a chronic alcoholic. Intern Med. 2010; 49(6):615-618.
39. Malhotra K, Ortega L. Central pontine myelinolysis with meticulous correction of hyponatraemia in chronic alcoholics BMJ Case Rep. 2013; 1-3; pii: bcr2013009970; doi: 10.1136/bcr-2013-009970.
40. Lodhi MU, Saleem TS, Kuzel AR, Khan D, Syed IA, et al. Beer potomania - a syndrome of severe hyponatremia with unique pathophysiology: case studies and literature review. Cureus. 2017; 9(12):e2000. doi: 10.7759/cureus.2000.
41. Levine JP, Stelnicki E, Weiner HL, Bradley JP, McCarthy JG. Hyponatremia in the postoperative craniofacial pediatric patient population: a connection to cerebral salt wasting syndrome and management of the disorder. Plast Reconstr Surg. 2001; 108(6):1501-1508.
42. Coleman M. Axon degeneration mechanisms: commonality amid diversity. Nat Rev Neurosci. 2005; 6(11): 889-898.
43. Pandit L. Differential diagnosis of white matter diseases in the tropics: An overview Ann Indian Acad Neurol. 2009; 12(1):12-21.
44. Lawson B, Silva J. [Central pontine myelinolysis and hyponatremia. Clinical case]. [Article in Spanish]. Rev Med Chil. 2001; 129(4):427-432.
45. Burneo J, Vizcarra D, Miranda H. [Central pontine myelinolysis and pregnancy: a case report and review of literature]. [in Spanish]. Rev Neurol. 2000; 30(11):1036-1040.

46. Corona G, Simonetti L, Giuliani C, Sforza A, Peri A. A case of osmotic demyelination syndrome occurred after the correction of severe hyponatraemia in hyperemesis gravidarum. BMC Endocr Disord. 2014; 14:34. doi: 10.1186/1472-6823-14-34.

47. Baldrighi M, Sainaghi PP, Bellan M, Bartoli E, Castello LM. Hyperosmolar state: a pragmatic approach to properly manage sodium derangements. Curr Diabetes Rev. 2018; 14(6): 534-541.

48. Bonkowsky JL, Filloux FM. Extrapontine myelinolysis in a pediatric case of diabetic ketoacidosis and cerebral edema. J Child Neurol. 2003; 18(2):144-147.

50. Stavroulopoulos A, Nakopoulou L, Xydakis AM, Aresti V, et al. Interstitial nephritis and nephrogenic diabetes insipidus in a patient treated with pemetrexed. Ren Fail.2010; 2(8) : 1000 - 1004.

51. Tajitsu M, Yamada T, Cao X, Fukui A, Nagai J, et al. Osmotic demyelination syndrome complicating diabetes with anti-glutamic acid decarboxylase antibodies], diabetes and Graves' disease: A case report. J Diabetes Investig. 2016; 7(1):130-131.

52. Arao K, Fujiwara T, Sakakura K, Wada H, Sugawara Y, et al. Hyponatremia as a predictor for worsening heart failure in patients receiving cardiac resynchronization therapy. Circ J. 2013; 77(1):116-122.

53. Jha AA, Behera V, Jairam A, Baliga KV. Osmotic demyelination syndrome in a normonatremic patient of chronic kidney disease. Indian J Crit Care Med. 2014; 18:609–611.

54. Sharma HS, Kiyatkin EA. Rapid morphological brain abnormalities during acute methamphetamine intoxication in the rat: an experimental study using light and electron microscopy. J Chem Neuroanat.2009; 37(1):18-32.

55. Guha K, Spießhöfer J, Hartley A, Pearse S, Xiu PY, Sharma R. The prognostic significance of serum sodium in a population undergoing cardiac resynchronisation therapy. Indian Heart J. 2017; 69(5):613-618.

56. Martinez-Cano JP, Cortes-Castillo V, Martinez-Villa J, et al. Dysnatremia among runners in a half marathon performed under warm and humid conditions. BMJ Open Sport Exerc Med. 2018; 4(1): e000351. doi: 10.1136/bmjsem-2018-000351. eCollection 2018.

57. Meinders AJ, Meinders AE. 2007. Hyponatremia during a long-distance run: due to excessive fluid intake. Ned Tijdschr Geneeskd 151(10): 581- 587.

58. Orakzai RH, Orakzai SH, Hasley PB. 2008. Treating hyponatremia: how slow is safe? Central pontine myelinolysis despite appropriate correction of hyponatremia. Eur J Intern Med 19: 29–31.

59. Facciorusso A, Amoruso A, Neve V, Antonino M et al. 2014. Role of vaptans in the management of hydroelectrolytic imbalance in liver cirrhosis. World J Hepatol. 6(11):793-799.

60. Yu C, Sharma N, Saab S. Hyponatremia: clinical associations, prognosis, and treatment in cirrhosis. Exp Clin Transplant. 2013; 11(1): 3-11.
61. Park M, Son HJ, Kim GS. 2019. Osmotic demyelination syndrome following hyponatremia-oriented management in liver transplant: A single center 20-year experience. Exp Clin Transplant. 17(4):540-545.
62. Guillaumin J, DiBartola SP. Disorders of sodium and water homeostasis. Vet Clin North Am Small Anim Pract. 2017; 47(2):293-312.
63. Burton AG, Hopper K. Hyponatremia in dogs and cats. J Vet Emerg Crit Care (San Antonio). 2019; 29(5):461-471.
64. Kleinschmidt-DeMasters BK, Norenberg MD. Rapid correction of hyponatremia causes demyelination: relation to central pontine myelinolysis. Science. 1981; 211(4486):1068-1070.
65. Illowsky BP, Laureno R. Encephalopathy and myelinolysis after rapid correction of hyponatraemia. Brain. 1987; 110 (Pt 4): 855-867.
66. Laureno R. Central pontine myelinolysis following rapid correction of hyponatremia. Ann Neurol. 1983; 13: 232-42.
67. Verbalis JG, Drutarosky MD. Adaptation to chronic hypoosmolality in rats. Kidney Int . 1988; 34: 351-360.
68. Thurston JH, Hauhart RE. 1987. Brain amino acids decrease in chronic hyponatremia and rapid correction causes brain dehydration: possible clinical significance. Life Sci. 1987; 29;40(26):2539-2542.
69. Thurston JH, Hauhart RE, Nelson JS. Adaptive decreases in amino acids (taurine in particular), creatine, and electrolytes prevent cerebral edema in chronically hyponatremic mice: rapid correction (experimental model of central pontine myelinolysis) causes dehydration and shrinkage of brain. Metab Brain Di. 1987; s 2(4):223-241.
70. Sugimura Y, Takagi H, Murase T, Hoshino S et al. Prevention of demyelination induced by rapid correction of hyponatremia in mice. Environmental Med. 2002; 46(2): 58–61.
71. Iwama S, Sugimura Y, Suzuki H, Suzuki H, et al. Time-dependent changes in proinflammatory and neurotrophic responses of microglia and astrocytes in a rat model of osmotic demyelination syndrome. Glia. 2011; 59(3):452-462
72. Bouchat J, Couturier B, Marneffe C, Gankam-Kengné F, et al. Regional oligodendrocytopathy and astrocytopathy precede myelin loss and blood-brain barrier disruption in a murine model of osmotic demyelination syndrome. Glia. 2018 ; 66 (3) : 606-622.
73. Bouchat J, Gilloteaux J, Suain V, Van Vlaender D et al. 2019. Ultrastructural analysis of thalamus damages in a mouse model of osmotic-induced demyelination. Neurotox Res. 2019; 36(1):144-162.

74. Nicaise C, Marneffe C, Bouchat J, Gilloteaux J. Osmotic demyelination: from oligodendrocyte to astrocyte perspective. Int J Med Sci. 2019; 20(5). pii: E1124. doi: 10.3390/ijms20051124.

75. Yuridullah R, Kumar V, Nanavati S, Singhal M, Chandran C. Clinical resolution of osmotic demyelination syndrome following overcorrection of severe hyponatremia. Case Rep Nephrol. 2019; 2019:1757656. doi: 10.1155/2019/1757656. eCollection 2019.

76. Menger H, Jarg T. 1999. Outcome of central pontine and extrapontine myelinolysis. J Neurol 246: 700-705.

77. Lambeck J, Hieber M, Dreßing A, Niesen WD. Central pontine myelinosis and osmotic demyelination syndrome. Dtsch Arztebl Int. 2019. 116 (35-36):600-606.

78. Tandukar S, Rondon-Berrios H. Treatment of severe symptomatic hyponatremia. Physiol Rep. 2019; 7(21):e14265. doi: 10.14814/phy2.14265.

79. Kiernan JA. Chromoxane cyanine R. II. Staining of animal tissues by the dye and its iron complexes. J Microsc. 1984; 134(Pt 1):25-39.

80. Stefanović D. Use of eriochrome cyanine R for routine histology and histopathology: an improved dichromatic staining procedure. Biotechnic & Histochem. 2015; 90 (6): 470-474.

81. Sternberger LA. Immunochemistry. New York: J Wiley & Sons. 1979.

82. Franklin K, Paxinos G. The Mouse Brain in Stereotaxic Coordinates. San Diego: Academic Press, 1997.

83. Bauer K. F. Elektronenmikroskopische Beobachtungen an der menschlichen Himrinde. Fortsch Neurol, Psych Grenzgebiete. 1968; 36: 274-309.

84. Vaughn JE, Skoff RP. Neuroglia in experimentally altered central nervous system. In: The Structure and Function of Nervous Tissue, vol. v (ed. G. H. Bourne), New York: Academic Press, 1972; pp.39-72.

85. Jones E.G. The Thalamus. vol II. Plenum Press New York-Springer Sciences and Business Media. 1985; pp.573-601.

86. Peters A, Palay SL, Webster H de F. The fine structure of the nervous system. 3rd edition. Alan Peters (ed.) New York: Oxford University Press. 1991.

87. Karasek M, Swiltosławski J, Zielińiska A. Ultrastructure of the central nervous system: the basics. Folia Neuropathol. 2004; 42 Suppl B: 1- 9.

88. Brodal P. The Central Nervous System. Fifth edition; New York; Oxford University Press. 2010.

89. Morell P. Myelin. New York: Plenum Publishing Co. 2e edition.1984.

90. Sango, K., Yamauchi, J., Ogata, T., Susuki, K. Myelin, Basic and Clinical Advances. In: Sango, K., Yamauchi, J., Ogata, T., Susuki, K. (eds.). Adv Exper Med Biol. 2019; Singapore: Springer.

91. Jones EG. Thalamic circuitry and thalamocortical synchrony. Phil Trans R Soc Lond B Biol Sci. 2002; 357(1428):1659-1673.
92. Jones EG. Thalamic organization and function after Cajal. Prog Brain Res. 2002; 136:333-57.
93. Bokor H, Frère SG, Eyre MD, Slézia A, Ulbert I, Lüthi A, Acsády L. Selective GABAergic control of higher-order thalamic relays. Neuron. 2005; 45(6):929-940.
94. Hammer S, Carrillo GL, Govindaiah G, Monavarfeshani A, Bircher JS, et al. Nuclei-specific differences in nerve terminal distribution, morphology, and development in mouse visual thalamus. Neural Dev. 2014; 16. 1-20.
95. Liu XB, Warren RA, Jones EG. Synaptic distribution of afferents from reticular nucleus in ventroposterior nucleus of cat thalamus. J Comp Neurol.1995; 352(2):187-202.
96. Simpson K, Wang Y, Lin RC. Patterns of convergence in rat zona incerta from the trigeminal nuclear complex: light and electron microscopic study. J Comp Neurol. 2008; 507 (4):1521-1341.
97. Yeterian EH, Pandya DN. Corticothalamic connections of the posterior parietal cortex in the rhesus monkey. J Comp Neurol 1985; 237(3):408-426.
98. Carpenter MB. Connectivity patterns of thalamic nuclei implicated in dyskinesia. Stereotact Funct Neurosurg. 1989; 52(2-4):79-119.
99. Lopez C, Blanke O. The thalamocortical vestibular system in animals and humans. Brain Res Rev. 2011; 67(1-2):119-146.
100. Olsen GM, Witter MP. Posterior parietal cortex of the rat: Architectural delineation and thalamic differentiation. J Comp Neurol. 2016; 524(18):3774-3809.
101. Gankam-Kengne F, Nicaise C, Soupart A, Boom A, et al. Astrocytes are an early target in osmotic demyelination syndrome. J Am Soc Nephrol. 2011; 22:1834-45.
102. Gankam-Kengne F, Couturier BS, Soupart A, Brion JP, Decaux G. Osmotic stress-induced defective glial proteostasis contributes to brain demyelination after hyponatremia treatment. J Am Soc Nephrol. 2017; 28: 1802-1813.
103. Gocht A, Lohler J. Changes in glial cell markers in recent and old demyelinated lesions in central pontine myelinolysis. Acta Neuropathol. 1990; 80: 46-58.
104. McCormick DA. Neurotransmitter actions in the thalamus and cerebral cortex. J Clin Neurophysiol. 1992; 9: 212 - 223.
105. Soupart A, Decaux G. Therapeutic recommendations for management of severe hyponatremia: current concepts on pathogenesis and prevention of neurologic complications. Clin Nephrol. 1996; 46(3):149-169.
106. Sood L, Sterns RH, Hix JK, Silver SM, Chen L. Hypertonic saline and desmopressin: a simple strategy for safe correction of severe hyponatremia. Am J Kidney Dis. 2013; 61(4):571-578.

107. Giuliani C, Peri A. Effects of hyponatremia on the brain. J Clin Med. 2014; 3(4):1163-77. doi: 10.3390/jcm3041163.

108. Sterns RH, Silver SM. Complications and management of hyponatremia. Curr Opin Nephrol Hypertens. 2016; 25(2):114-119.

109. Adler S, Verbalis JG, Meyers S, Simplaceanu E, Williams DS. Changes in cerebral blood flow and distribution associated with acute increases in plasma sodium and osmolality of chronic hyponatremic rats. Exp Neurol. 2000; 163: 63-71.

110. Baker EA, Tian Y, Adler S, Verbalis JG. Blood-brain barrier disruption and complement activation in the brain following rapid correction of chronic hyponatremia. Exp Neurol. 2000; 165 (2): 221-230.

111. Rojiani AM, Prineas JW, Cho ES. Electrolyte-induced demyelination in rats. 1. Role of the blood-brain barrier and edema. Acta Neuropathol. 1994; 88(4):287-92.

112. Rojiani AM, Cho ES, Sharer L, Prineas JW. Electrolyte-induced demyelination in rats. 2. Ultrastructural evolution. Acta Neuropathol. 1994; 88 (4): 293-299.

113. Hochstrasser T, Rühling S, Hecher K, Fabisch KH, et al. Stereological investigation of regional brain volumes after acute and chronic cuprizone-induced demyelination. Cells. 2019; 8 (9):1024. 2-17 doi: 10.3390/cells8091024.

114. Chow BW, Gu C. Gradual suppression of transcytosis governs functional blood-retinal barrier formation. Neuron. 2017; 93(6): 1325–1333. e3. doi: 10.1016/j.neuron.2017.02.043.

115. Chow BW, Nuñez V, Kaplan L, Granger AJ et al. Caveolae in CNS arterioles mediate neurovascular coupling. Nature. 2020; 579 (7797): 106–110.

116. Ono S, Inoue K, Mannen T, Mitake S, Shirai T et al. Intracytoplasmic inclusion bodies of the thalamus and the substantia nigra, and Marinesco bodies in myotonic dystrophy: a quantitative morphological study. Acta Neuropathol. 1989; 77(4): 350-356.

117. Sato H, Sato M. Ultrastructural morphology of thalamic cytoplasmic inclusion bodies in El mouse. Exp Neurol. 1986; 93 (1): 160-167.

118. Arcelli P, Rassoni F, Regondi MC, De Biasi S, Spreafico R. GABAergic neurons in mammalian thalamus: A marker of thalamic complexity? Brain Res Bull.1997; 42 (1): 27-37.

119. Sherman SM, Guillery RW. On the actions that one nerve cell can have on another: Distinguishing “drivers” from “modulators”. Proc Natl Acad Sci USA. 1998; 95 (12) 7121-7126.

120. Sherman SM. Thalamic relay functions. Prog Brain Res. 2001; 134: 51-69.

121. Sherman SM, Guillery RW. The role of the thalamus in the flow of information to the cortex. Philos Trans R Soc Lond B Biol Sci. 2002; 357(1428):1695-1708.

122. García-Cabezas MÁ, John YJ, Barbas H, Zikopoulos B. 2016. Distinction of neurons, glia and endothelial cells in the cerebral cortex: an algorithm based on cytological features. Front Neuroanat. 2016; 10: 107. doi: 10.3389/fnana.2016.00107.
123. Bopp R, Holler-Rickauer S, Martin KAC, Schuhknecht GFP. An ultrastructural study of the thalamic input to layer 4 of primary motor and primary somatosensory cortex in the mouse. J Neurosci. 2017; 37(9): 2435–2448.
124. Mullen RJ, Buck CR, Smith AM. NeuN, a neuronal specific nuclear protein in vertebrates. Development. 1992; 116(1):201–211.
125. Alekseeva OS, Gusel'nikova VV, Beznin GV, Korzhevskii DE. [Prospects of the nuclear protein NeuN application as an index of functional state of the vertebrate nerve cells] Zh Evol Biokhim Fiziol. 2015; 51(5):313–323.
126. Gusel'nikova VV, Korzhevskiy DE. NeuN as a neuronal nuclear antigen and neuron differentiation marker. Acta Naturae. 2015; 7: 42-47.
127. Duan W, Zhang YP, Hou Z, Huang C, et al. Novel insights into NeuN: from neuronal marker to splicing regulator. Mol Neurobiol. 2016; 53(3):1637–1647.
128. You H, Kim YI, Im SY, Suh-Kim H et al. Immunohistochemical study of central neurocytoma, subependymoma, and subependymal giant cell astrocytoma J Neurooncol. 2005; 74(1):1-8.
129. Wolf HK, Buslei R, Schmidt-Kastner R, Schmidt-Kastner PK et al. NeuN: a useful neuronal marker for diagnostic histopathology J Histochem Cytochem. 1996; 44: 1167–1171.
130. Darlington PJ, Goldman JS, Cui QL, Antel JP, Kennedy TE. Widespread immunoreactivity for neuronal nuclei in cultured human and rodent astrocytes. J Neurochem. 2008; 104. P. 1201–1209.
131. Kim KK, Adelstein RS, Kawamoto S. Identification of neuronal nuclei (NeuN) as Fox-3, a new member of the Fox-1 gene family of splicing factors. J Biol Chem. 2009; 284: 31052–31061.
132. Kim KK, Kim YC, Adelstein RS, Kawamoto S. Fox-3 and PSF interact to activate neural cell-specific alternative splicing. Nucleic Acids Res 2011; 39; 3064–3078.
133. Maxeiner S, Glassmann A, Kao HT, Schilling K. The molecular basis of the specificity and cross-reactivity of the NeuN epitope of the neuron-specific splicing regulator, Rbfox3. Histochem Cell Biol 2014; 141(1): 43-55.
134. Nickerson JA, Krochmalnic G, Wan KM, Penman S. 1989. Chromatin architecture and nuclear RNA. Proc Natl Acad Sci USA. 1989; 86(1):177-181.
135. Ma B, Day JP, Phillips H, Slootsky B, et al. Deletion of the hemopexin or heme oxygenase-2 gene aggravates brain injury following stroma-free hemoglobin-induced intracerebral hemorrhage. J Neuroinflammation 2016; 13:26.

136. Hakim NH, Kounishi T, Alam AH, Tsukahara T, Suzuki H. Alternative splicing of Mef2c promoted by Fox-1 during neural differentiation in P19 cells. Genes Cells. 2010; 15(3):255-267.

137. Dent MA, Segura-Anaya E, Alva-Medina J, Aranda-Anzaldo A. NeuN/Fox-3 is an intrinsic component of the neuronal nuclear matrix. FEBS Lett. 2010;584(13):2767–2771.

138. Dredge BK, Jensen KB. NeuN/Rbfox3 nuclear and cytoplasmic isoforms differentially regulate alternative splicing and nonsense-mediated decay of Rbfox2. PLoS One 2011; 6(6): e21585. doi: 10.1371/journal.pone.0021585

139. Thiry M, Lepoint A, Goessens G. Re-evaluation of the site of transcription in Ehrlich tumour cell nucleoli. Biol Cell. 1985; 54, 57–64.

140. Thiry M, Goessens G. Distinguishing the sites of pre-rRNA synthesis and accumulation in Ehrlich tumor cell nucleoli. J. Cell Sci. 1991; 99,759 -767.

141. Schwarzacher HG, Wachtler F. The functional significance of nucleolar structures. Ann Genet. 1991; 34(3-4):151-160.

142. Schwarzacher HG, Wachtler F. The nucleolus. Anat Embryol (Berl). 1993; 188(6): 515-536.

143. Thiry M, Cheutin T, O'Donohue MF, Kaplan H, Ploton D. Dynamics and three-dimensional localization of ribosomal RNA within the nucleolus. RNA. 2000; 6: 1750–1761.

144. Fakan S, Hernandez-Verdun D. 1986. The nucleolus and the nucleolar organizer regions. Biol Cell. 2002; 56(3):189-205.

145. Thiry M, Thiry-Blaise L. In situ hybridization at the electron microscope level: an improved method for precise localization of ribosomal DNA and RNA. Eur J Cell Biol. 1989; 50, 235–243.

146. Derenzini M, Thiry M, Goessens G. Ultrastructural cytochemistry of the mammalian cell nucleolus. J Histochem Cytochem. 1990; 38(9): 1237-56.

147. Biggiogera M, Malatesta M, Abolhassani-Dadras et al. Revealing the unseen: the organizer region of the nucleolus. J Cell Sci. 2001; 114: 3199-3205.

148. Thiry M, Goessens G. Where, within the nucleolus, are the rRNA genes located? Exp Cell Res. 1992; 200 (1):1-4.

149. Angelier N, Tramier M, Louvet E, Coppey-Moisan M, Savino TM, et al. Tracking the interactions of rRNA processing proteins during nucleolar assembly in living cells. Mol Biol Cell.2005; 16(6):2862-2871.

150. Raska I, Shaw PJ, Cmarko D. New insights into nucleolar architecture and activity. Int Rev Cytol. 2006; 255: 177–234.

151. Gitler D, Xu Y, Kao HT, Lin D, et al. Molecular determinants of synapsin targeting to presynaptic terminals. J Neurosci. 2004; 24(14):3711-20.

152. Buratti E, Baralle FE Influence of RNA secondary structure on the pre-mRNA splicing process. Mol Cell Biol. 2004; 24 (24): 10505-10514. doi: 10.1128/MCB.24.24.10505-10514.2004
153. Li Q, Lee JA, Black DL. Neuronal regulation of alternative pre-mRNA splicing. Nature Rev Neurosci 2007; 8 (11): 819 - 831.
154. Gu J, Chen F, Chu D, Lu Y, Iqbal K, Gong CX, Liu F. Rbfox3/NeuN regulates alternative splicing of tau exon 10. J Alzheimers Dis. 2018; 66(4):1695-1704.
155. Burns ER, Soloff BL, Hanna C, Buxton DF. Nuclear pocket associated with the nucleolus in normal and neoplastic cells. Cancer Res. 1971; 31: 159–65.
156. Buxton DF. Nuclear pocket associated with the nucleolus in normal and neoplastic cells. Cancer Res. 1971; 31: 159–65.
157. Dupuy-Coin AM, Moens P, Bouteille M. Three-dimensional analysis of given cell structures: nucleolus, nucleoskeleton, and nuclear inclusions. Methods Achiev. Exp. Pathol. 1986; 12:1–25.
158. Bourgeois CA, Hubert J. Spatial relationship between the nucleolus and the nuclear envelope: Structural aspects and functional significance. Int Rev Cytol.1988; 111: 1- 52.
159. Wang N, Butler JP, Ingber DE. Mechanotransduction across the cell surface and through the cytoskeleton. Science. 1993; 260 (5111):1124-7.
160. Coene ED, Van Oostveldt P, Willems K, van Emmelo J, De Potter CR. BRCA1 is localized in cytoplasmic tube-like invaginations in the nucleus. Nature Genet. 1997; 16: 122–124.
161. Fricker M, Hollinshead M, White N, Vaux D. Interphase nuclei of many mammalian cell types contain deep, dynamic, tubular membrane-bound invaginations of the nuclear envelope. J Cell Biol. 1997; 136(3): 531-544.
162. Maniotis AJ, Chen CS, Ingber DE. 1997. Demonstration of mechanical connections between integrins, cytoskeletal filaments, and nucleoplasm that stabilize nuclear structure. Proc Natl Acad Sci USA 1997; 94(3): 849-854.
163. Pederson T. The plurifunctional nucleolus. Nucleic Acids Res. 1998; 26(17):3871-3876.
164. Pederson T. The nucleolus. Cold Spring Harb Perspect Biol. 2011; 3(3). pii: a000638.
165. Johnson N, Krebs M, Boudreau R, Giorgi G, et al. Actin-filled nuclear invaginations indicate degree of cell de-differentiation. Differentiation. 2003;71: 414–424.
166. Lammerding J, Lee RT. Mechanical properties of interphase nuclei probed by cellular strain application. Methods Mol Biol. 2009; 464: 13 - 26.
167. Mirre C, Lammerding J. Mechanics of the nucleus. Comprehensive Physiology. 2011; 1(2), 783–807.

168. Mukherjee RN, Chen P, Levy DL. Recent advances in understanding nuclear size and shape. Nucleus. 2016; 7 (2): 167-186

169. Drozdz MM, Vaux DJ. Shared mechanisms in physiological and pathological nucleoplasmic reticulum formation. Nucleus. 2017;8(1):34-45.

170. Delpire E, Duchêne C, Goessens G, Gilles R. Effects of osmotic shocks on the ultrastructure of different tissues and cell types. Exp Cell Res. 1985; 160(1):106-16.

171. Bourgeois CA, Hernandez-Verdun D, Hubert J, Bouteille M. Silver staining of NORs in electron microscopy. Exp Cell Res.1979;123(2):449-452.

172. Clubb BH, Locke M. 3T3 cells have nuclear invaginations containing F-actin. Tissue Cell. 1998; 30: 684–691.

173. Alam SG, Lovett D, Kim DI, Roux KJ, Dickinson RB, Lele TP. The nucleus is an intracellular propagator of tensile forces in NIH 3T3 fibroblasts. J Cell Sci. 2015; 128: 1901-1911.

174. Poplawski GHD, Kawaguchi R, Van Niekerk E, Lu P et al. Injured adult neurons regress to an embryonic transcriptional growth state. Nature. 2020; 581(7806):77-82.

175. Valentin G. Repertorium für Anatomie und Physiologie, 1, Verlag von Veit und Comp. Berlin, 1836; 1–293.

176. Schwann T. Mikroskopische Untersuchungen über die Übereinstimmung in der Struktur und dem Wachsthum der Theiren und Pflanze. Verlag der Sander'schen Buchhandlung (Berlin). 1839; pp. 1–270.

177. Montgomery TH. Comparative cytological studies, with especial regard to the morphology of the nucleolus. J. Morph 1898; 15, 265–582.

178. Goessens G. The nucleolar fibrillar centres in various cell types in vivo or in vitro. Cell Tissue Res. 1976; 173(3):315-24.

179. Goessens G. Nucleolar ultrastructure during reversible inhibition of RNA synthesis in chick fibroblasts cultivated in vitro. J Ultrastruct Res. 1978; 65(1):83-89.

180. Goessens G. Relations between fibrillar centres and nucleolus-associated chromatin in Ehrlich tumour cells. Cell Biol Int Rep. 1979; 3(4):337-343.

181. Goessens G. Localisation of nucleolus-organizing regions in interphase cells. Cell Tissue Res. 1979; 200(1):159-161.

182. Bouteille M, Hernandez-Verdun D. Localization of a gene: the nucleolar organizer. Biomedicine. 1979; 30(6): 282-287.

183. Goessens G. Nucleolar structure. Int Rev Cytol. 1984; 87: 107–158.

184. Radoux D, Lepoint A, Goessens G. [Cytological study of nucleoli and nucleolar organizers during inhibition of RNA synthesis]. In French. Bull Assoc Anat (Nancy). 1980; 64(185):259-266.

185. Mirre C, Knibiehler B. A re-evaluation of the relationships between the fibrillar centres and the nucleolus-organizing regions in reticulated nucleoli: ultrastructural organization, number and distribution of the fibrillar centres in the nucleolus of the mouse Sertoli cell. J Cell Sci. 1982; 55:247-59.

186. Mirre C, Stahl A. Ultrastructural organization, sites of transcription and distribution of fibrillar centres in the nucleolus of the mouse oocyte. J Cell Sci. 1981; 48:105-126.

139-148

187. Ploton D, Thiry M, Menager M, Lepoint A et al. Behaviour of nucleolus during mitosis. A comparative ultrastructural study of various cancerous cell lines using the Ag-NOR staining procedure. Chromosoma. 1987; 95(2):95-107.

188. Chelidze PV, Mdivani TV, Dzidziguri DV, Cherkeziia EO, et al. [The 3-dimensional organization of the nucleolus and the nucleolus organizer regions in differentiated cells. II. The reticular, vacuolized and nucleolonemal nucleoli of hepatocytes from the intact mouse liver and of hepatocytes stimulated to proliferation as a result of partial hepatectomy]. [Article in Russian]. Tsitologiia. 1992; 34(9):17-25.

189. Chelidze PV, Dzidziguri DV, Zarandiia MA, Georgobiani NM et al. [The 3-dimensional organization of the nucleolus and nucleolus-organizer regions of differentiated cells. IV. The structural and functional heterogeneity of the nucleoli in the epithelium of the proximal nephron in the mouse]. [Article in Russian]. Tsitologiia. 1993; 35(10): 3-12.

190. Chelidze PV, Dzidziguri DV, Kintsurashvili LN, Kir'ianov GI, et al. [The dependence of the 3-dimensional organization and length of the nucleolonema in the hepatocyte nucleoli of normal and regenerating rat livers on the nucleosome structure of the intranucleolar chromatin]. [Article in Russian].Tsitologiia. 1995; 37(9-10): 859-871.

191. Jamison JM, Gilloteaux J, Adrian M, Summers JL. Effect of ethidium on the morphology, antiviral activity and subcellular distribution of poly r(A-U). Cell Biol Int. 1993; 17(12):1091-105

192. Krabill K, Jamison JM, Gilloteaux J, Summers JL. Subcellular localization and antiviral activity of carminic acid/poly r(A-U) combinations. Cell Biol Int 1993; 17(10):919-34.

193. Thiry M, Jamison JM, Gilloteaux J, Summers JL et al. Ultrastructural nucleolar alterations induced by an ametantrone/polyr(A-U) complex. Exp Cell Res. 1997; 236(1): 275-284.

194. Thiry M, Ploton D, Menager M, Goessens G. Ultrastructural distribution of DNA within the nucleolus of various animal cell lines or tissues revealed by terminal deoxynucleotidyl transferase. Cell Tissue Res. 1993; 271(1):33-45.

195. Thiry M, Scheer U, Goessens G. Localization of DNA within Ehrlich tumour cell nucleoli by immunoelectron microscopy. Biol Cell. 1988; 63(1): 27-34.

196. Thiry M, Scheer U, Goessens G. Localization of nucleolar chromatin by immunocytochemistry and in situ hybridization at the electron microscopy level. Electron Microsc. Rev. 1991; 4: 85–110.

197. Schwarzacher HG, Mosgoeller W. Ribosome biogenesis in man: current views on nucleolar structures and function. Cytogenet Cell Genet. 2000; 91(1-4):243-252.
198. Boisvert FM, van Kőningsbruggen S, Navascués J, Lamond AI. The multifunctional nucleolus. Nat Rev Mol Cell Biol. 2007; 8(7): 574-585. https://doi.org/10.1038/nrm2184
199. Mattaj IW, Tollervey D, Séraphin B. 1993. Small nuclear RNAs in messenger RNA and ribosomal RNA processing. FASEB J 1993; 7(1):47-53.
200. Scheer U, Thiry M, Goessens G. Structure, function and assembly of the nucleolus. Trends Cell Biol. 1993; 3(7):236- 241.
201. Trendelenburg MF, Zatsepina OV, Waschek T, Schlegel W et al. Multiparameter microscopic analysis of nucleolar structure and ribosomal gene transcription. Histochem Cell Biol. 1996; 106(2):167-192.
202. Vandelaer M, Thiry M, Goessens G. AgNOR proteins from morphologically intact isolated nucleoli. Life Sci. 1999; 64(22): 2039 – 2047.
203. Savino TM, Gébrane-Younès J, De Mey J, Sibarita JB, Hernandez-Verdun D. Nucleolar assembly of the rRNA processing machinery in living cells. J Cell Biol. 2001; 53(5):1097-1110.
204. Hernandez-Verdun D, Roussel P, Thiry M, Sirri V, Lafontaine DL. The nucleolus: structure/function relationship in RNA metabolism. Wiley Interdiscip Rev 2010; RNA 1(3): 415-31.
205. Jamison JM, Gilloteaux J, Perlaky L, Thiry M, et al. Nucleolar changes and fibrillarin redistribution following apatone treatment of human bladder carcinoma cells. J Histochem Cytochem. 2010; 58(7): 635-651.
206. Gilloteaux j, Jamison JM, Neal D, Summers JL. Synergistic antitumor cytotoxic actions of ascorbate and menadione on human prostate (DU145) cancer cells in vitro: nucleus and other injuries preceding cell death by autoschizis. Ultrastruct Pathol. 2014; 38(2):116-140.
207. Gilloteaux J, Jamison JM, Arnold D, Summers JL. Autoschizis: A Mode of Cell Death of Cancer Cells Induced by a Prooxidant Treatment In Vitro and In Vivo. In: J.A. Radosevich (ed): Apoptosis and BeyonD. New York: Wiley-Blackwell. doi: 10.1002/9781119432463; 2018; Ch 28; p. 583-694.
208. Hadjiolov AA. The nucleolus and ribosome biogenesis. Vienna: Springer Verlag, 1985.
209. Grummt I. The nucleolus—guardian of cellular homeostasis and genome integrity. Chromosoma. 2013; 122(6):487-97.
210. Day RN, Periasamy A, Schaufele F. Fluorescence resonance energy transfer microscopy of localized protein interactions in the living cell nucleus. Methods 2001; 25(1):4-18.
211. Fatica A, Tollervey D. Making ribosomes. Curr. Opin. Cell Biol. 14, 313–318.

212. Lagace TA, Ridgway ND. The rate-limiting enzyme in phosphatidylcholine synthesis regulates proliferation of the nucleoplasmic reticulum. Mol Biol Cell. 2005; 16: 1120–30.
213, Russell J, Zomerdijk JC. RNA-polymerase-I-directed rDNA transcription, life and works. Trends Biochem Sci. 2005; 30(2):87-96.
214. Louvet E, Tramier M, Angelier N, Hernandez-Verdun D. Time-lapse microscopy and fluorescence resonance energy transfer to analyze the dynamics and interactions of nucleolar proteins in living cells. Methods Mol Biol 2008; 463:123-135.
215. Szczepanowska K, Senft K, Heidler J, Herholz M, Kukat A, et al. A salvage pathway maintains highly functional respiratory complex I. Nature Commun. 2020; 11(1):1643. doi: 10.1038/s41467-020-15467-7.
216. Barron KD, Means ED, Larsen E. Ultrastructure of retrograde degeneration in thalamus of rat: 1. Neuronal somata dendrites. J Neuropathol Exp. Neurol.1973; 32 (2): 218–244.
217. Brooks GA, Dubouchaud H, Brown, M, Sicurello JP, Butz CE. Role of mitochondrial lactate dehydrogenase and lactate oxidation in the intracellular lactate shuttle. Proc Natl Acad Sci USA. 1999; 96:1129–1134.
218. Pérez-Escuredo J, Van Hée VF, Sboarina M, Falces J, Payen VL, Pellerin L, Sonveaux P. Monocarboxylate transporters in the brain and in cancer. Biochim Biophys Acta. 2016; 1863(10):2481-2497.
219. Bak LK, Walls AB, Schousboe A, Waagepetersen HS. Astrocytic glycogen metabolism in the healthy and diseased brain. J Biol Chem. 2018; 293:7108-7116.
220. Díaz-García CM, Mongeon R, Lahmann C, Koveal D, Zucker H, Yellen G. Neuronal stimulation triggers neuronal glycolysis and not lactate uptake. Cell Metab. 2017; 26(2):361-374.e4. doi: 10.1016/j.cmet.2017.06.021.
221. Yellen G. Fueling thought: Management of glycolysis and oxidative phosphorylation in neuronal metabolism. J Cell Biol. 2018; 217(7):2235-2246.
222. Zhu J, Li P, Zhou YG, Ye J. Altered energy metabolism during early optic nerve crush injury: Implications of Warburg-like aerobic glycolysis in facilitating retinal ganglion cell survival. Neurosci Bull. 2020; 36(7):761-777.
223. Lui L, Lowe T. Small nucleolar RNAs and RNA-guided post-transcriptional modification. Essays Biochem 2013; 54: 53-77.
224. Vincent WS. Structure and chemistry of nucleoli. Int. Rev. Cytol. 1955; 4: 269–298.
225. Porter KR. Observations on a submicroscopic basophilic component of cytoplasm. J. Exp. Med. 1953; 97, 727–750.
226. Palade GE, Porter KR. Studies on the endoplasmic reticulum. J. Exp. Med. 1954; 100, 641–656.
227. Watson ML. The nuclear envelope; its structure and relation to cytoplasmic membranes. J Biophys Biochem Cytol. 1955; 25: 257–270.

228. Walter P, Gilmore R, Muller M, Blobel G. The protein translocation machinery of the endoplasmic reticulum. Philos Trans R. Soc Lond B Biol Sci. 1982; 300: 225–228.

229. Franke WW. Nuclear envelopes. Structure and biochemistry of the nuclear envelope. Phil Trans R Soc Lond B. 1974; 268, 67–93.

230. Franke WW. Structure, biochemistry, and functions of the nuclear envelope. Int Rev Cytol. 1974; Suppl. 4, 71–236.227.

231. Gilloteaux J, Kashouty R, Yono N. The perinuclear space of pancreatic acinar cells and the synthetic pathway of zymogen in Scorpaena scrofa L.: Ultrastructural aspects. Tissue Cell. 2008; 40(1): 7-20.

232. Goler-Baron V, Selitrennik M, Barkai O, Haimovich G, et al. Transcription in the nucleus and mRNA decay in the cytoplasm are coupled processes. Genes Dev. 2008; 22(15):2022–2027.

233. Hartenian E, Glaunsinger BA. Feedback to the central dogma: cytoplasmic mRNA decay and transcription are interdependent processes. Crit Rev Biochem Mol Biol 2019; 54(4): 385–398.

234. George R, Griffin JW. The proximo-distal spread of axonal degeneration in the dorsal columns of the rat. J Neurocytol. 1994; 23(11):657-67.

235. Koshinaga M, Whittemore SR. The temporal and spatial activation of microglia in fiber tracts undergoing anterograde and retrograde degeneration following spinal cord lesion. J Neurotrauma 1995; 12 (2): 209–222.

236. Freeman MR. Signaling mechanisms regulating Wallerian degeneration Curr Opin Neurobiol. 2014; 27: 224-231.

237. Geden MJ, Deshmukh M. Axon degeneration: context defines distinct pathways. Curr Opin Neurobiol. 2016; 39: 108-115. doi: 10.1016/j.conb.2016.05.002.

238. Buss A, Schwab ME. Sequential loss of myelin proteins during Wallerian degeneration in the rat spinal cord. Glia. 2003; 42(4):424-432.

239. Adalbert R, Nógrádi A, Szabó A, Coleman MP. The slow Wallerian degeneration gene in vivo protects motor axons but not their cell bodies after avulsion and neonatal axotomy. Eur J Neurosci. 2006; 24 (8): 2163–8.

240. Guo S, Tjärnlund-Wolf A, Deng W, Tejima-Mandeville E, et al. Comparative transcriptome of neurons after oxygen-glucose deprivation: Potential differences in neuroprotection versus reperfusion. J Cereb Blood Flow Metab. 2018; 38(12):2236-2250.

241. Sanders P, De Keyser J. Janus faces of microglia in multiple sclerosis. Brain Res Rev. 2007; 54(2):274-285.

242. Takefuji S, Murase T, Sugimura Y, Takagishi Y, et al. Role of microglia in the pathogenesis of osmotic-induced demyelination. Exp Neurol. 2007; 204(1):88-94.

243. Ghosh N, DeLuca GC, Esiri MM. Evidence of axonal damage in human acute demyelinating diseases. J Neurol Sci. 2004; 222: 29-34.
244. Kumar V, Abbas A, Aster J. Cellular Responses to Stress and Toxic Insults: Adaptation, Injury, and Death. In: Robbins Basic Pathology, 10th Edition, Elsevier. 2017; Chapter 2: p. 3-23.
245. Kumar V, Abbas A, Fausto N, Aster J. In: Robbins and Cotran: Pathologic Basis of Disease, 8th ed, Philadelphia: Elsevier-Saunders. 2010; p. 5-16.
246. Peña CE. Intracytoplasmic neuronal inclusions in the human thalamus. Light-microscopic, histochemical, and ultrastructural observations. Acta Neuropathol. 1980; 52(2):157-159.
247. Aikawa H, Suzuki K, Iwasaki Y. Ultrastructural observation on the thalamic neuronal inclusion in young mice. Acta Neuropathol. 1983; 59(4):316-318.
248. Ono S, Inoue K, Mannen T, Mitake S. et al. Intracytoplasmic inclusion bodies of the thalamus and the substantia nigra, and Marinesco bodies in myotonic dystrophy: a quantitative morphological study. Acta Neuropathol.1989; 77, 350–356.
249. Takahashi H, Ohama E, Ikuta F. Are bunina bodies of endoplasmic reticulum origin? An ultrastructural study of subthalamic eosinophilic inclusions in a case of atypical motor neuron disease. Acta Pathol Jpn. 1991 ; 41 (12): 889-894.
250. Cummings JF, de Lahunta A, Summers BA, Mohammed HO, et al. Eosinophilic cytoplasmic inclusions in sporadic equine motor neuron disease: an electron microscopic study. Acta Neuropathol. 1993; 85(3):291-7.
251. Brabec V, Kleinwächter V, Vetterl V. 1997. Bioelectrochemistry of Biomacromolecules. In: Bioelectrochemistry of Biomacromolecules, G Lenaz and G Milazzo (eds). Basel: Birkhäuser Verlag, p 1-104. doi: https://doi.org/10.1007/978-3-0348-9179-0
252. Brengues M, Teixeira D, Parker R. Movement of eukaryotic mRNAs between polysomes and cytoplasmic processing bodies. Science. 2005; 310(5747): 486-489.
253. Bhattacharyya SN, Habermacher R, Martine U, Closs EI, Filipowicz W. Stress-induced reversal of microRNA repression and mRNA P-body localization in human cells. Cold Spring Harb Symp Quant Biol. 2006; 71: 513-521.
254. Pillai RS, Bhattacharyya SN, Filipowicz W. Repression of protein synthesis by miRNAs: how many mechanisms? Trends Cell Biol. 2007; 17(3): 118-126.
255. Parker R, Sheth U. P bodies and the control of mRNA translation and degradation. Mol Cell. 2007; 25(5): 635-646.
256. Balagopal V, Parker R. Polysomes, P bodies and stress granules: states and fates of eukaryotic mRNAs. Curr Opin Cell Biol. 2009; 21(3): 403-408.
257. Von Roretz C, Di Marco S, Mazroui R, Gallouzi IE. Turnover of AU-rich-containing mRNAs during stress: a matter of survival. Wiley Interdiscip Rev RNA. 2011; 2(3):336-347.

258. Decker CJ, Parker R. P-bodies and stress granules: possible roles in the control of translation and mRNA degradation. Cold Spring Harb Perspect Biol. 2012; 4(9):a012286. doi: 10.1101/cshperspecta012286.

261. Bhattacharyya A, Oppenheim RW, Prevette D, Moore BW et al. S100 is present in developing chicken neurons and Schwann cell and promotes motor neuron survival in vivo. J Neurol. 1992; 23 (4): 451-466.

259. Anderson KI, Wang YL, Small JV. Coordination of protrusion and translocation of the keratocyte involves rolling of the cell body. J Cell Biol. 1996; 134 (5): 1209–1218.

260. Kumar, A., Maitra A, Sumit M, Ramaswamy S, Shivashankar GV. 2015. Actomyosin contractility rotates the cell nucleus. Sci Rep 2015; 4, 3781 https://doi.org/10.1038/srep03781.

261. Bard F, Bourgeois CA, Costagliola D, Bouteille M. Rotation of the cell nucleus in living cells: a quantitative analysis. Biol Cell. 1985; 54(2):135-42.

262. Fung LC, De Boni U. Modulation of nuclear rotation in neuronal interphase nuclei by nerve growth factor, by gamma-aminobutyric acid, and by changes in intracellular calcium. Cell Motil Cytoskeleton. 1988; 10(3):363-73.

263. Paddock SW, Albrecht-Buehler G. Rigidity of the nucleus during nuclear rotation in 3T3 cells. Exp Cell Res. 1988; 175(2):409-413.

264. Park PC, De Boni U. Dynamics of nucleolar fusion in neuronal interphase nuclei in vitro: association with nuclear rotation. Exp Cell Res. 1991; 197(2): 213-221.

265. Gundersen GG, Worman HJ. Nuclear Positioning. Cell. 2013; 152(6): 1376-1389. doi.org/10.1016/j.cell.2013.02.031.

266. Yang Z, Voke PR. Large-eddy simulation of boundary-layer separation and transition at a change of surface curvature. J Fluid Mech. 2001; 439: 305 – 333.

267. Garrett SJ, Peake N. The stability and transition of the boundary layer on a rotating sphere. J Fluid Mech. 2002; 456: 199 – 218.

268. Wu MH, Wen CY, Yen RH, Weng MC et al. Experimental and numerical study of the separation angle for flow around a circular cylinder at low Reynolds number. J Fluid Mech. 2004; 515, 233-260.

269. Pijush K. Kundu PK, Cohen IM, Dowling DR. Fluid Mechanics. In: Pijush K. Kundu, Ira M. Cohen and David R. Dowling (eds), Fifth Edition, Amsterdam: Elsevier/ Academic Press. 2012; p 171-196; 473-540 and 541-620. https://doi.org/10.1016/C2009-0-63410-3

270. Salehi MA, Mazaheri S, Kazeminezhad MH. Pressure distribution around a near-wall circular cylinder subjected to steady current. 18th Marine Industries Conference (MIC2016), 2016; https://www.researchgate.net/publication/312024837-324.e28. doi: 10.1016/j.cell.2020.03.050

271. Wiggins A. Fluid flow about immersed bodies flow stream U drag = pressure + friction. Part B – In: White F. ed. Fluid Mechanics, 7th ed. F. White F. New York: McGrawHill Co. 2016; Ch 9: p. 609-700.
272. Riback JA, Zhu L, Ferrolino MC, Tolbert M et al. Composition-dependent thermodynamics of intracellular phase separation.Nature. 2020; 581(7807): 209-214.
273. Sanders DW, Kedersha N, Lee DSW, Strom AR et al. Competing Protein-RNA interaction networks control multiphase intracellular organization. Cell. 2020; 181(2):306-24. https://doi.org/10.1016/j.cell.2020.03.050
274. Wicke F, Moreitz S, Weidauer S. Osmotic demyelination syndrome due to severe hyponatremia mimicking hypoxic encephalopathy. Fortschr Neurol Psychiatr. 2017; 85(4):212-215.
275. Li Q, Weiland A, Chen X, Lan X et al. Ultrastructural characteristics of neuronal death and white matter injury in mouse brain tissues after intracerebral hemorrhage: coexistence of ferroptosis, autophagy, and necrosis. Front Neurol 2018; 9, 581. https://doi.org/10.3389/fneur.2018.00581
276. Vogel FS, Bouldin TW. The Nervous System. In: Rubin E, Farber JL, editors. Pathology. 2nd ed. Philadelphia: J.B. Lippincott. 1994; Chapter 28: p 1373-1455.
277. Zhan J, Mann T, Joost S, Behrangi N, Frank M, Kipp M. The Cuprizone Model: Dos and Do Nots. Cells. 2020; 9(4). pii: E843. doi: 10.3390/cells9040843.
278. Powers JM, McKeever PE. Central pontine myelinolysis. An ultrastructural and elemental study. J Neurol Sci. 1976; 29: 65- 81.278.
279. Norenberg MD, Leslie KO, Robertson AS. Association between rise in serum sodium and central pontine myelinolysis. Ann Neurol. 1982 ; 11 :128–135.
280. Popescu BF, Bunyan RF, Guo Y, Parisi JE et al. Evidence of aquaporin involvement in human central pontine myelinolysis. Acta Neuropathol Commun. 2013 ; 1:40. doi: 10.1186/2051-5960-1- 40.
281. Ghadially FN. Ultrastructural Pathology of the Cell and Matrix. 4th edition. Boston: Butterworth-Heinemann 1997. pp.30-31.
282. Sullivan AA, Chervin RD, Albin RL. Parkinsonism after correction of hyponatremia with radiological central pontine myelinolysis and changes in the basal ganglia. J Clin Neurosci. 2000; 7(3):256-259.
283. Giuliani C, Peri A. Effects of hyponatremia on the brain. J Clin Med. 2014 Oct 28;3(4):1163-1377.

Acknowledgements

JP B was supported by grants T.0023.15 from the Belgian “Fonds de la Recherche Scientifique Médicale” and the Belgian Foundation “Recherche Alzheimer/ Stichting Alzheimer Onderzoek” (14001; Fund Aline). This ultrastructural study was performed in the Electron Microscope facility of the” Plateforme Technologique Morphologie - Imagerie” of the Université de Namur with the technical assistance of Corry Charlier and Valérie Suain.

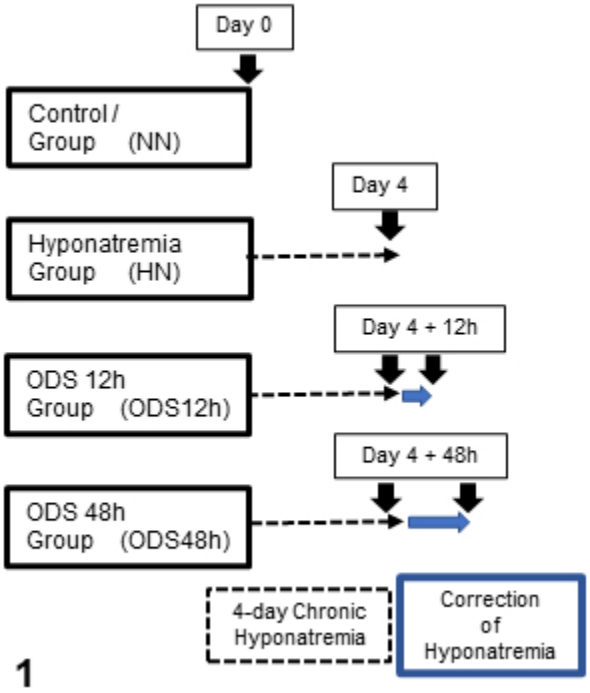

Figure 1: Experiments performed on 4 groups of 2 mice excepted for ODS 48 h which included 3 mice. Normonatremic mice (NN) from group 1 were sacrificed at day 0 (arrow) while uncorrected hyponatremic mice (HN) were sacrificed 4 days after the induction of hyponatremia (arrow). ODS mice were sacrificed as groups 3 and 4, at respectively 12 and 48 h post correction (arrows).

89x100mm (96 x 96 DPI)

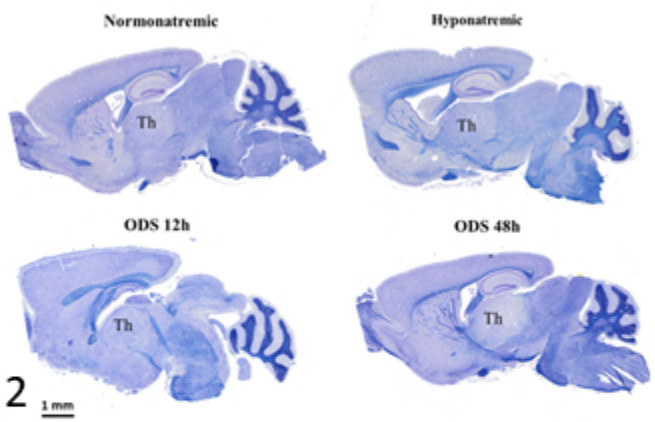

Figure 2. Pane from sagittal sections of normatremia (NN) or Sham, hyponatremia (HN), 12h after correction of hyponatremia (ODS12h) and 48h after correction of hyponatremia (ODS48h) mice brains. All stained with hemalum and eriochrome cyanine and ODS 48h best revealed thalamus (th) as demyelination zone.

89x100mm (96 x 96 DPI)

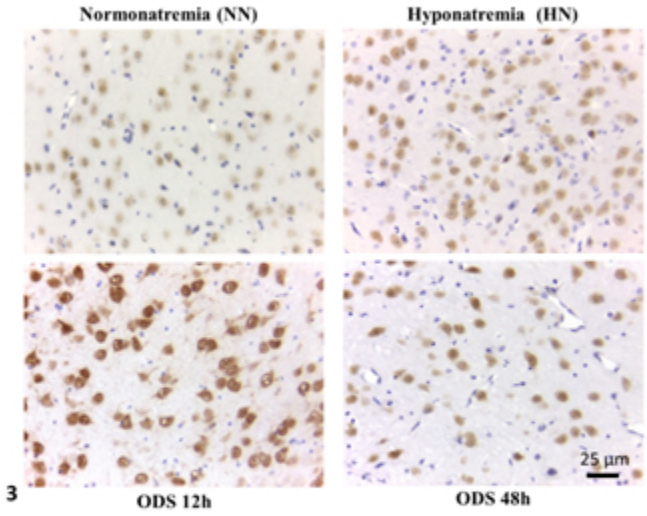

Figure 3: NeuN immunolabeled paraffin sections of NN-, HN-, ODS12h- and ODS48h-treated thalamic ventral posterior nucleus. Scales in ODS48h main micrograph is for all micrographs.

89x100mm (96 x 96 DPI)

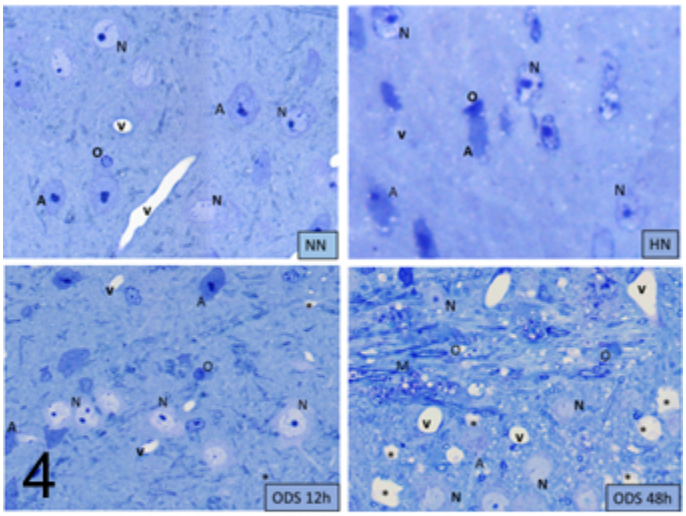

Figure 4: Pane illustrating 1µm-thick epoxy thick sections of NN, HN, ODS12h and ODS48h from the ventral posterior nucleus thalamic region. Examples of some neuron cell bodies (N), astrocytes (A), oligodendrocytes (O), and myelinated tracts (M) are indicated throughout; in ODS12h and 48h sections, myelinolysis neuropil cavities are marked (*) while other clear spaces, lined by endothelial cells are small blood vessels. Scales equal 10 µm.

89x100mm (96 x 96 DPI)

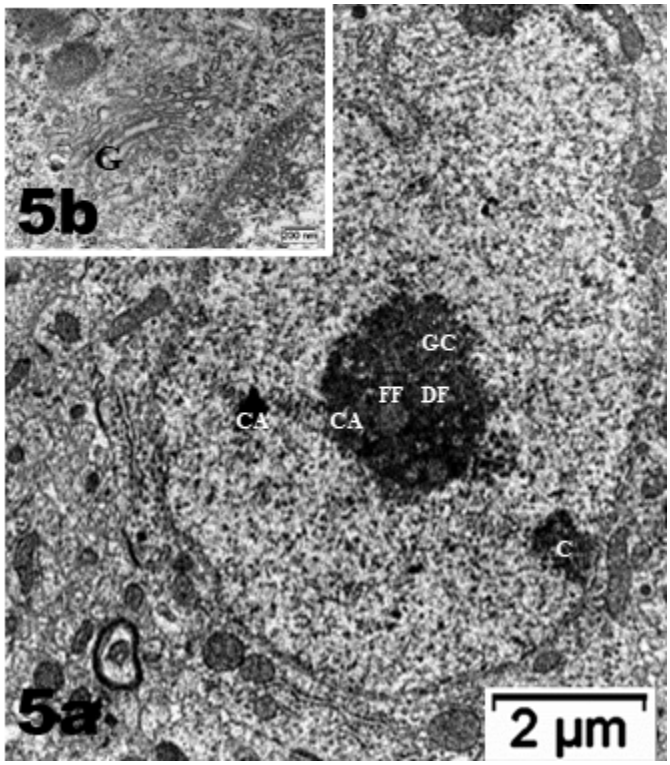

Figure 5 A-D: Selected views of NN murine neuron cell bodies of the latero-ventral thalamic nuclei and enlarged aspects of nucleoli. A, C and D: Euchromatic nuclei with slightly indented envelopes with quasi centrally-located nucleoli with their 3 main highly active transcriptional featured components: CA: chromatin associated, part of C: chromatin, as associated with the inner nuclear envelope; DF: dense fibrillar, FF: fine fibrillar region accompanied by its cloud of ribonucleoprotein transcript products as granules i.e. small and large ribosomal and other RNAs (Granular Component as GC). B: enlarged Golgi zone of A.

89x100mm (96 x 96 DPI)

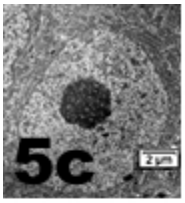

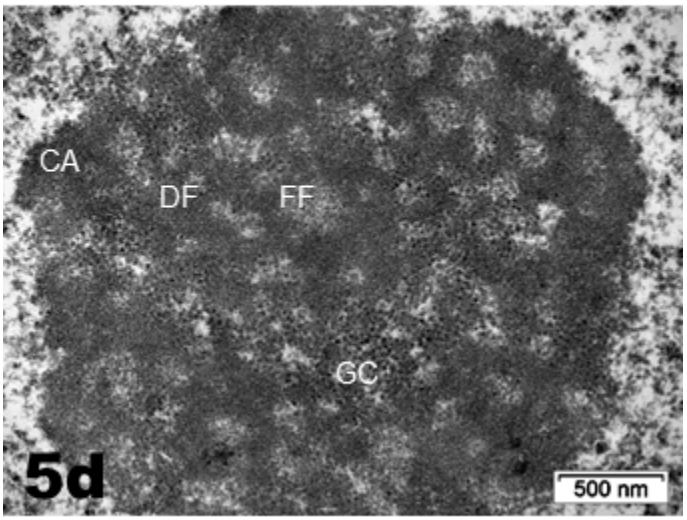

see above

89x100mm (96 x 96 DPI)

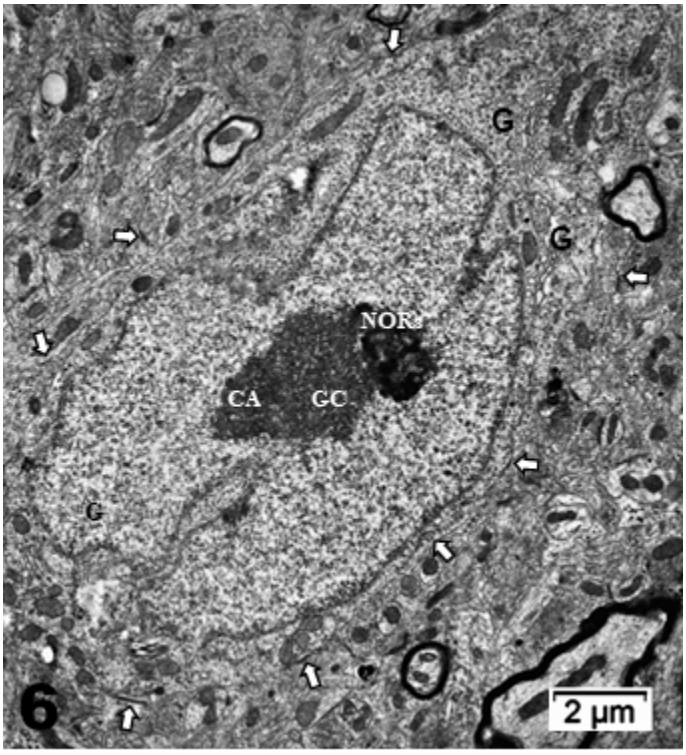

Figure 6: Neuron cell body of NN murine latero-ventral thalamic region. A: Euchromatic nucleus with deeply indented envelope reaching, in its central zone, the large nucleolus and its 3 main aligned components indicating high transcription activities: CA: chromatin associated, GC: granular center (ribonucleoprotein components); CA+GC both forming nucleolar organizer centers or NORs; DF: dense fibrillar and FF: fine fibrillar region. G: Golgi apparatus; axo-somatic synapses are marked by small white arrows. Compare this micrograph with that of Figure 11 A.

89x100mm (96 x 96 DPI)

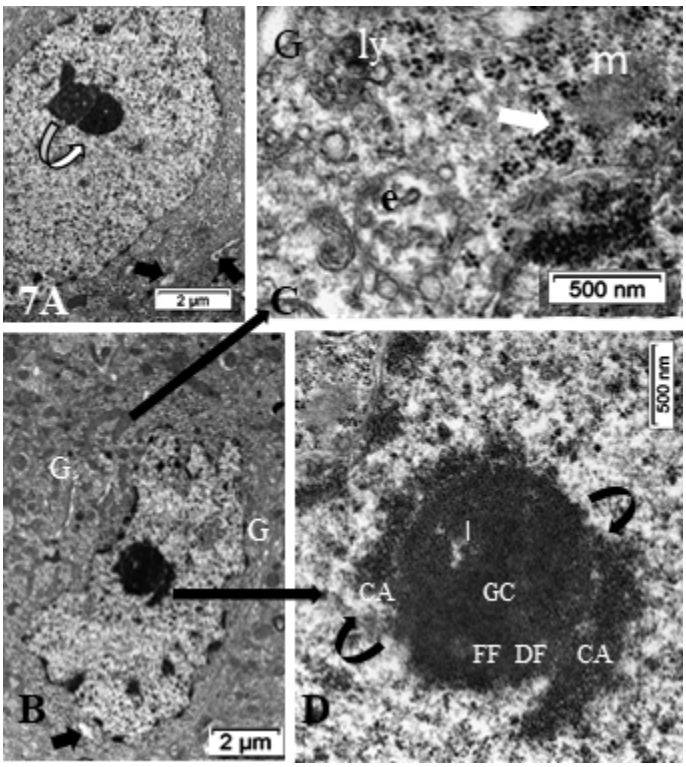

Figure 7 A-D: HN neuron cell bodies of the parenchyma of the latero-ventral thalamic parenchyma showing the nucleus topology change (A-B) as well as the nucleolus. A and B segregation of the nucleolus CA/DF regions from GC component (curved arrows in A and D) suggestive of a reduced or stoppage in transcriptional activities because accumulated ribonucleoproteins (GC) amassed separated from the chromatin (CA) becoming concentric of GC, and its extension as dense fibrillar (DF). The fine fibrillar region (pale circles in nucleolus depicting transcription (FF) is absent. In the GC mass, interstices are formed (I) as CA leaves the nucleolus. Example of perikaryon of B in C revealed scattered free polysomes but none attached to adjacent endoplasmic reticulum (white arrow), part of Golgi zone, an endosome (e) and many coated vesicles, maybe forming autophagosomes (ly); a peculiar fuzzy osmiophilic mass (m) deposits among the cytosol. Note discrete intercellular spaces formed by [Na+] depletion.

89x100mm (96 x 96 DPI)

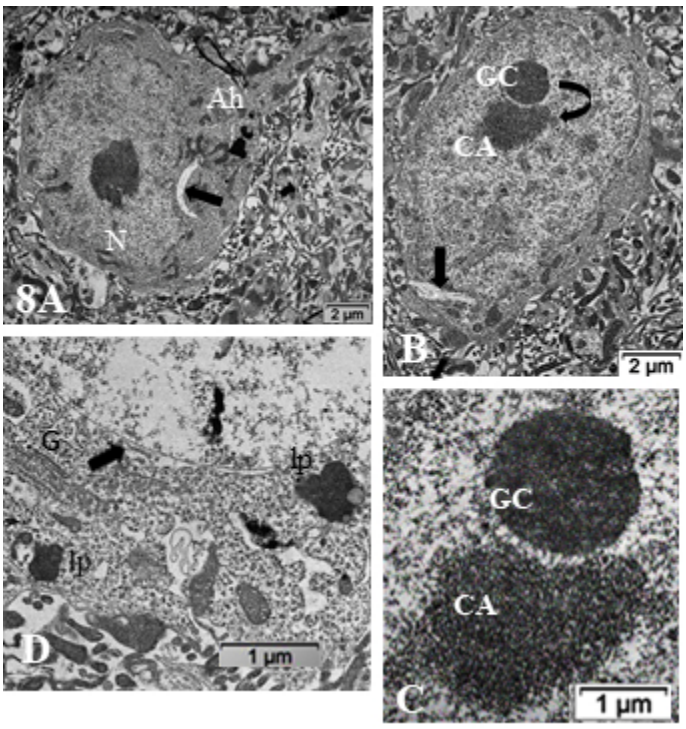

Figure 8 A-D: ODS12h nerve cell bodies in the demyelinated region, ventrolateral nuclei of the mouse thalamus. Nucleus shows a prominent nucleolus where both chromatin- associated (CA) and granular center (GC) are recognized and completed separated from one another (curved arrow) along with other perikaryal damages (arrows in A-C); Ah: axon hillock. In D: damages consist in ER membrane's degradations, including those of the nucleus envelope (arrowed), the endoplasm and Golgi apparatus (G); lipofuscin bodies (lp). CNS parenchyma is the degraded neuropil in A-B and D.

89x100mm (96 x 96 DPI)

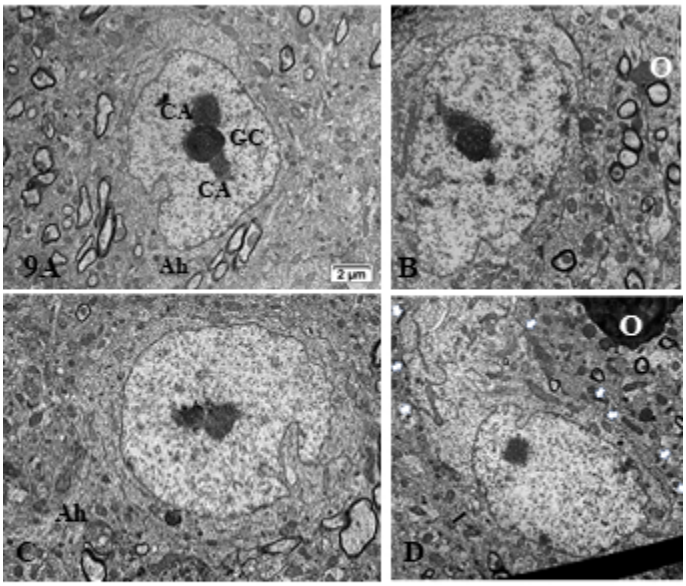

Figure 9 A-D: Pane with ODS12h nerve cell bodies preserved, adjacent to the demyelinated zone of the ventrolateral thalamus showing typical euchromatic nuclei with prominent nucleoli where components, although evident in all the featured micrographs, do not form NORs and are centrally placed and somewhat segregated into CA and GC regions. In B and D, highly contrasted oligodendrocyte section parts in the surrounded neuropil (O). In D, small white arrows display examples of axo-somatic synaptic sectors. Ah: axon hillock; G: Golgi zone; arrow shows autophagosome. Scale in A is the same for B-D.

89x100mm (96 x 96 DPI)

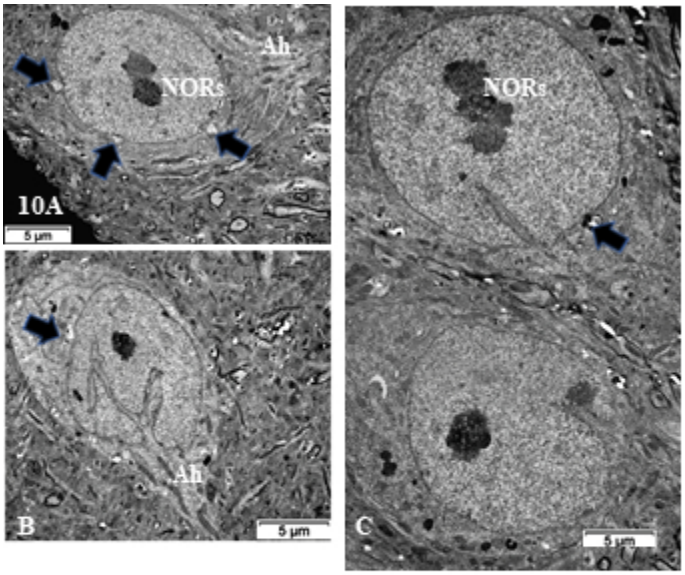

Figure 10 A-C: TEM pane with ODS 48h thalamus euchromatic nerve cell body aspects among the neuropil where damages can still be viewed as myelin damages remained throughout. Prominent nerve cell bodies with nucleolus have regained round with indentations and highly contrasted but active nucleolus organization (NORs) have reorganized into all active parts as those described in NN cells. Arrows indicate nucleus envelope damages. Ah: axon hillock.

89x100mm (96 x 96 DPI)

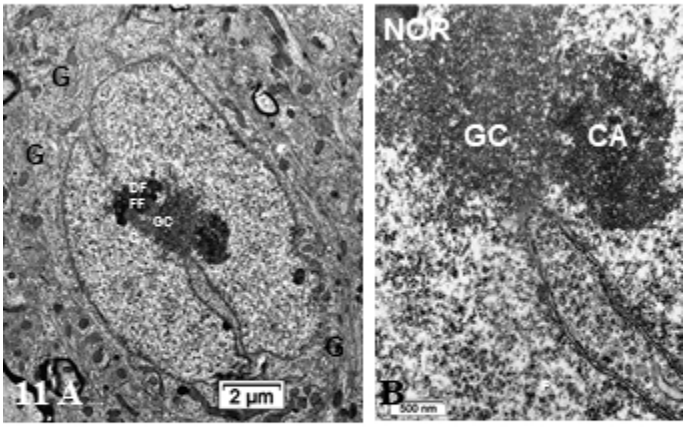

Figure 11 A-B: Pane of one ODS 48h nerve cell body of murine thalamus showing similar aspect nucleus as found in some NN cells (see Fig 6), including a similar display of its envelope indent. The prominent nucleolus is revealed with NORs and components with a huge cloud of ribonucleoproteins (GC) and the chromatin associated (CA). Golgi apparatus encircles the nucleus in the reactivated perikaryon. Neuropil surroundings still reveal discrete to evident demyelinated axon damages as remnant whorls or evident interfascicular cavities or voids. B: Enlarged aspect of the A nucleus depicting nucleolus where ribonucleoprotein reach the adjacent, envelope indent whose neuroplasm content is loaded by numerous polysomes, aimed at translational activities.

89x100mm (96 x 96 DPI)

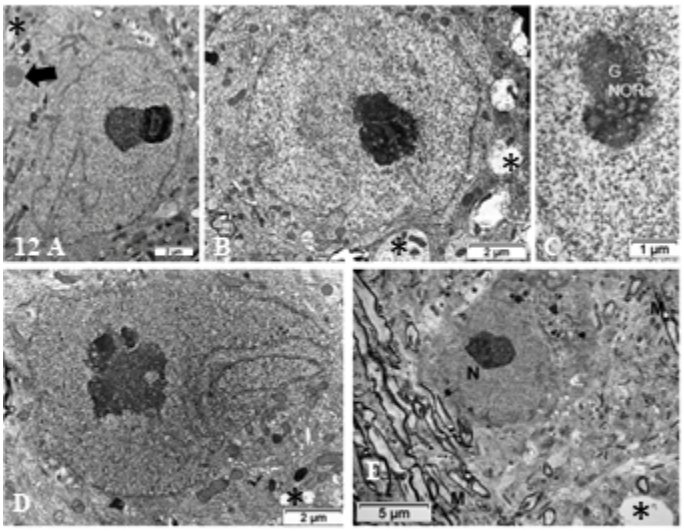

Figure 12 A-E: Pane of ODS 48h nerve cell bodies of murine thalamus containing several examples of nucleus profiles (A-D), associated prominent activated nucleoli revealing many NORs, and adjacent neuropil with damaged axons whose removal of myelin have left intercellular spaces or voids (stars in B, D and E). A peculiar neuroplasm deposit is arrowed in A (see Figures 14-15). C: enlarged nucleolus with NORs: G: granular component; CA: chromatin associated chromatin. E: Neuron adjacent to a myelinated nerve bundle; star: intercellular cavity left from myelinolysis.

89x100mm (96 x 96 DPI)

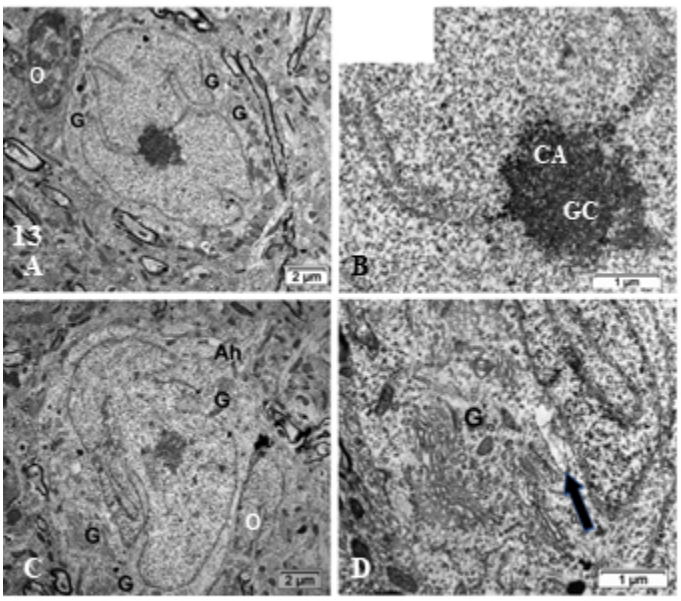

Figure 13 A-D: TEM of ODS48h ventro-lateral thalamus neuron cell bodies with the enlarged perikaryon. Both depict long deep, twisted indents of the nucleus envelope as if reaching the active nucleolus, as in Figure 11A viewing many organelles i.e. G: Golgi, ly: lysosomes, ER and mitochondria. Ah: Axon hillock region; CA: chromatin associated to nucleolus, GC: granular center; O; oligodendrocyte; Arrow in D indicates fragile nucleus envelope endoplasm defects.

89x100mm (96 x 96 DPI)

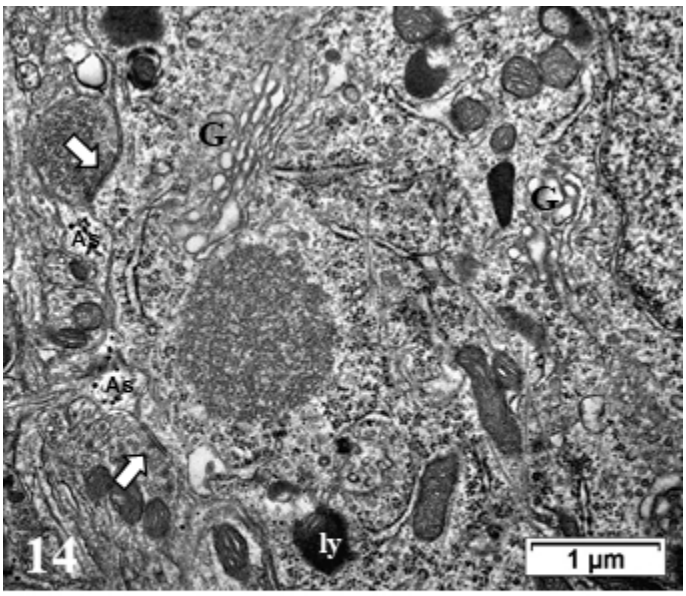

Figure 14: TEM aspect of the enlarged neuron perikaryon of Figure 11A with many organelles i.e. G: Golgi, ly: lysosomes, ER and mitochondria along with a peculiar round fibro-particulate aggregate. N; nucleus. Some of the axo-somatic synapses are indicated by open arrows; G: Golgi, ly: lysosomes, ER and mitochondria along with a peculiar round fibro-particulate aggregate. N; nucleus; axo-somatic synapse (arrowed). As: Astrocyte parts with beta-glycogen granules.

89x100mm (96 x 96 DPI)

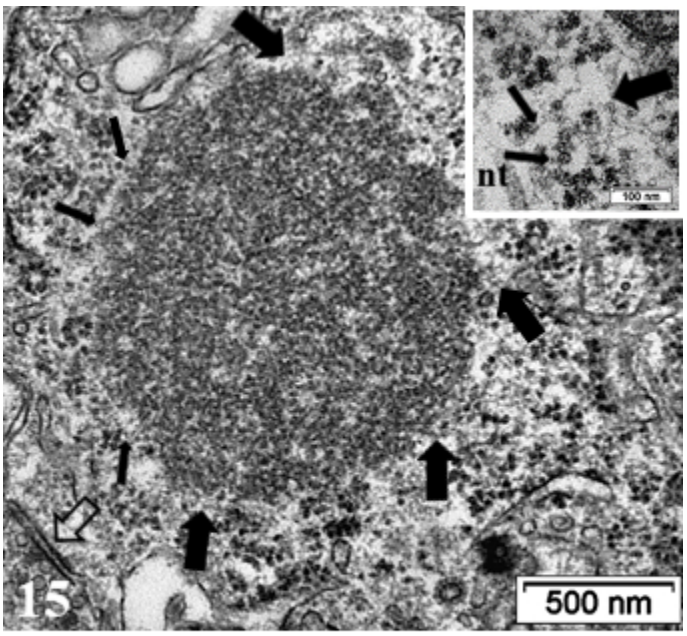

Figure 15: Detailed view of the fibro-particulate aggregate where sticking out filamentous extensions are marked by thick arrows and thin arrows indicate particulate parts. Axo-somatic synapse (open arrow). Insert: Exhibit of the edge of the aggregate somewhat concealed components indicating that threads emerging out of it are from 4-5 nm in thickness (wide arrows) with mRNA – polysome structures (thin arrows); nt: neurotubule.

89x100mm (96 x 96 DPI)